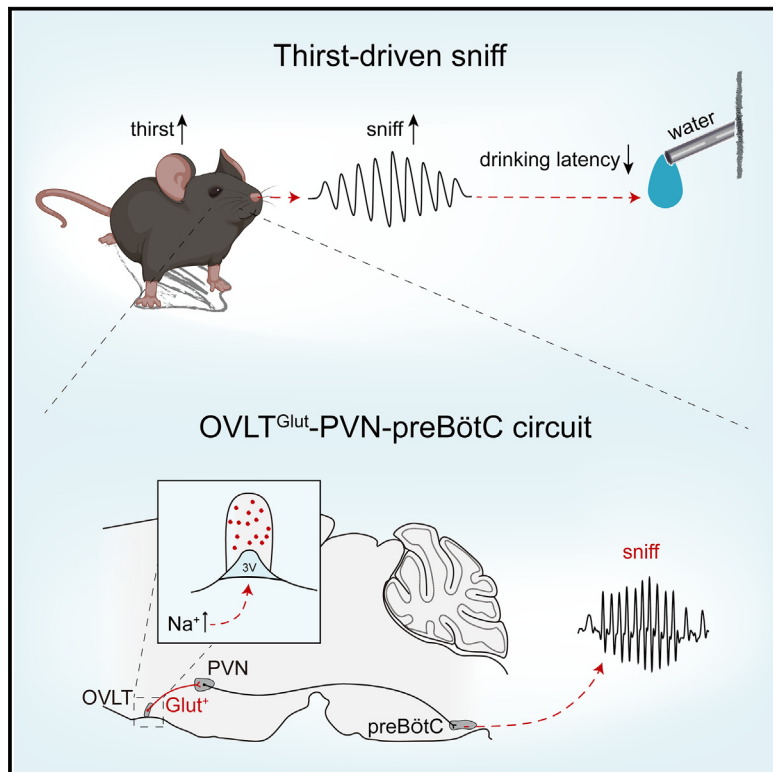


## Activation of glutamatergic neurons in the organum vasculosum of the lamina terminalis induces thirst-driven sniffing

### Graphical abstract



### Authors

Wei He, Luo Shi, Ziteng Yue, ..., Yongqiang Chen, Fang Yuan, Sheng Wang

### Correspondence

yuanfang@hebmu.edu.cn (F.Y.), wangsheng@hebmu.edu.cn (S.W.)

### In brief

He et al. report that activation of glutamatergic neurons in the organum vasculosum of the lamina terminalis induces thirst-driven sniffing behaviors through the paraventricular nucleus of the hypothalamus to preBötzinger complex circuit, thereby enhancing water-seeking efficiency. This circuit represents a crucial pathway that integrates internal thirst signals with specific respiratory motor outputs.

### Highlights

- Hypertonic stimulation induces robust exploratory sniffing behaviors
- Stimulation of OVLT<sup>Glut</sup> neurons increases sniffing by mobilizing the PVN-preBötC circuit
- Hypertonic solution-induced sniffing is reduced by ablating preBötC-projecting PVN neurons



## Article

# Activation of glutamatergic neurons in the organum vasculosum of the lamina terminalis induces thirst-driven sniffing

Wei He,<sup>1,4</sup> Luo Shi,<sup>1,4</sup> Ziteng Yue,<sup>1</sup> Ke Zhao,<sup>1</sup> Xiaoyi Wang,<sup>1</sup> Kailin Wang,<sup>1</sup> Xinyi Jing,<sup>1</sup> Shangyu Bi,<sup>1</sup> Tianjiao Deng,<sup>1</sup> Xue Zhao,<sup>1</sup> Xiaochen Tian,<sup>1</sup> Xiangchen Ma,<sup>1</sup> Yongqiang Chen,<sup>1</sup> Fang Yuan,<sup>1,2,\*</sup> and Sheng Wang<sup>1,2,3,5,\*</sup>

<sup>1</sup>Department of Neurobiology, Hebei Medical University, Shijiazhuang 050017, China

<sup>2</sup>Hebei Key Laboratory of Neurophysiology, Shijiazhuang, China

<sup>3</sup>Key Laboratory of Neural and Vascular Biology, Ministry of Education, Shijiazhuang, China

<sup>4</sup>These authors contributed equally

<sup>5</sup>Lead contact

\*Correspondence: yuanfang@hebmu.edu.cn (F.Y.), wangsheng@hebmu.edu.cn (S.W.)

<https://doi.org/10.1016/j.celrep.2025.115254>

## SUMMARY

Sniffing is a specialized respiratory behavior that enables rodents to localize and track objects in their environment. The organum vasculosum of the lamina terminalis (OVLT) is critically involved in the regulation of thirst and water intake, yet its role in controlling thirst-driven exploratory sniffing behaviors remains unclear. This study demonstrates that hypertonic stimulation significantly increases sniffing and activates OVLT glutamatergic (OVLT<sup>Glut</sup>) neurons. Photostimulation of both OVLT<sup>Glut</sup> neurons and their axon terminals within the paraventricular nucleus of the hypothalamus (PVN) induces robust sniffing. Furthermore, ablation of PVN neurons projecting to the preBötzinger complex not only reduces the sniffing time induced by photostimulation of OVLT<sup>Glut</sup> neurons projecting to the PVN but also prolongs the drinking latency. These findings identify the OVLT<sup>Glut</sup>-PVN-preBötzinger complex circuit as a pivotal regulator of thirst-driven sniffing, providing insights into the neural mechanisms underlying thirst and exploratory behavior.

## INTRODUCTION

Active sensing enables animals to selectively sample spatial regions and temporal epochs, regulating stimulus intensity and dynamics to optimize sensory processing.<sup>1,2</sup> Behavioral strategies for sampling odors are remarkably complex in mammals, typically termed sniffing.<sup>3</sup> Sniffing, together with whisking, is rhythmic orofacial motor activity that enables rodents to localize and track objects in their environment.<sup>4</sup> Additionally, sniffing, which is commonly mobilized during motivated and social behaviors,<sup>5</sup> has been extensively investigated in a variety of species, including dogs,<sup>6</sup> rodents<sup>7,8</sup> and humans,<sup>6,9</sup> among others.<sup>10</sup>

In rodents, sniffing is defined as rapid, rhythmic respiration that involves the coordinated action of nasal and respiratory muscles to modulate airflow through the nasal cavity.<sup>11</sup> Despite its importance, the neural mechanisms underlying the generation of sniffing remain poorly understood. However, studies suggest that brainstem respiratory centers, such as the preBötzinger complex (preBötC), nucleus tractus solitarius (NTS), retrotrapezoid nucleus, and lateral parafacial nucleus, are involved in the generation of sniffing.<sup>11–13</sup> Additionally, cortical areas, including the insular and infralimbic cortices, can induce an increase in respiration frequency through electrical stimulation, mimicking exploratory sniffing.<sup>14</sup> In humans, sniffing, regardless of the presence of an odorant, has been shown to activate neuronal circuits primarily

in the piriform cortex of the temporal lobe and in the medial and posterior orbitofrontal gyri of the frontal lobe.<sup>15,16</sup> Furthermore, electrical stimulation of the lateral hypothalamus (LH) induces exploratory behaviors and high-frequency sniffing,<sup>17</sup> indicating the broad involvement of multiple brain regions in sniffing. However, the specific neural circuitry underlying motivation-driven exploratory sniffing remains largely uncharacterized.

Thirst, a physiological state triggered by dehydration or a decrease in blood volume, drives coordinated water-seeking and consumption behaviors across a wide array of animal species.<sup>18</sup> In the mammalian brain, the detection of fluid imbalance is primarily mediated by the circumventricular organs located in the lamina terminalis, which subsequently initiate thirst and regulate water intake.<sup>19</sup> Two critical structures in this process are the subfornical organ (SFO) and the organum vasculosum lamina terminalis (OVLT), both of which are essential for sensing internal fluid status and modulating drinking behavior via their downstream neural targets.<sup>20</sup> Specifically, in rodent brains, the OVLT has been identified as the predominant structure involved in thirst regulation, with its glutamatergic neurons (referred to as OVLT<sup>Glut</sup> neurons) playing a central role in this process.<sup>20,21</sup> Nevertheless, the precise contribution of OVLT<sup>Glut</sup> neurons to the generation of sniffing behavior, which is hypothesized to play a role in regulating water seeking, and the underlying neural circuit mechanisms remains poorly understood.



In this study, we hypothesize that stimulation of OVLT<sup>Glut</sup> neurons induces sniffing and facilitates water-seeking behaviors. Employing multidisciplinary approaches, our findings demonstrate that activation of OVLT<sup>Glut</sup> neurons triggers thirst-driven sniffing through an OVLT<sup>Glut</sup>-paraventricular nucleus (PVN)-pre-BötC circuit.

## RESULTS

### Hypertonic stimulation induces sniffing

Thirst has been shown to elicit robust exploratory behaviors in mice.<sup>18</sup> Following the detection of scents, mice typically exhibit exploratory sniffing, a specialized respiratory pattern characterized by breathing frequency (BF) exceeding 4 Hz. This frequency is significantly elevated compared to the resting BF of approximately 1–3 Hz.<sup>5</sup> To determine whether the exploratory sniffing is intensified during hyperosmotic-induced thirst, we employed whole-body plethysmography (WBP) in conjunction with video recordings to monitor sniffing in conscious C57BL/6J mice (Figure 1A).

Mice were acclimated to the plethysmograph chambers for 2 h daily over a period of 5 days, during which they had *ad libitum* access to food and water. On the sixth day, they received an intraperitoneal (i.p.) injection of hypertonic NaCl (2 M, 8 µL/g body weight) to induce thirst, followed by sniffing measurements. Control mice received an equivalent volume of saline. For both groups, measurements were conducted for 1 h on day 6, during which time the mice had sensory but no physical access to water (Figure 1B). Our findings demonstrated that hypertonic stimulation, as opposed to saline, induced notable sniffing (Figures 1C and 1D), with a manifestation of an increase in both BF (Figures 1E and 1F) and peak inspiratory flow (PIF) (Figures 1G and 1H), in tandem with nose and head movements associated with exploration (Video S1). The intensified sniffing activity predominantly occurred within approximately 30 min after injection of hypertonic NaCl and diminished gradually thereafter. Additionally, the cumulative duration of sniffing episodes over the course of 1 h was significantly extended the hypertonic group compared to the control group (Figures 1I and 1J). Based on these observations, hypertonic stimulation induces pronounced exploratory sniffing in mice.

### OVLT<sup>Glut</sup> neurons mediate thirst-driven exploratory sniffing

The hypothalamic lamina terminalis, including the median preoptic nucleus (MnPO), SFO, and OVLT, plays a pivotal role in regulating thirst by integrating information on blood volume, osmolarity, and hormonal levels.<sup>20,22,23</sup> Accumulated evidence has shown that activation of neurons in the MnPO, SFO, and OVLT can drive thirst and water-intake behaviors.<sup>23</sup> In our study, systemic hyperosmotic stimulation led to increased cFos expression in neurons across all these three regions (Figures S1A–S1G), supporting their activation in response to osmotic challenges.

Studies have reported that the OVLT, rather than the MnPO or SFO, is the primary site for the regulation of [Na<sup>+</sup>]-dependent sympathetic output.<sup>24,25</sup> Additionally, lesions in the OVLT markedly reduce water intake compared to those in the SFO.<sup>26,27</sup>

with OVLT ablation causing a decrease of ~70% in water intake following hypertonic NaCl injection in mice.<sup>26</sup> Furthermore, the SFO regulates water intake through its axonal connections to the OVLT.<sup>28,29</sup> Based on these findings, we focused on the OVLT as a potential regulator in thirst-driven exploratory sniffing.

We extended our investigations to further examine the histomolecular phenotypes of these cFos<sup>+</sup> neurons in the OVLT. Combined application of RNAscope *in situ* hybridization and immunohistochemical staining demonstrated that 79.1% of cFos<sup>+</sup> neurons were glutamatergic (Figures S1H–S1J). Next, we aimed to determine the temporal correlation between the activation of OVLT<sup>Glut</sup> neurons and the onset of sniffing behaviors. To this end, fiber photometry was utilized to measure the dynamic Ca<sup>2+</sup> signals of OVLT<sup>Glut</sup> neurons by injecting a virus encoding GCaMP6s into the OVLT of satiated Vglut2-Cre mice, followed by immunohistochemical staining to confirm the expression of GCaMP6s (Figure 2A). The integration of WBP and *in vivo* fiber photometry recordings enabled the concurrent monitoring of sniffing onset and the activation level of OVLT<sup>Glut</sup> neurons. Our observations revealed that after injection of hypertonic NaCl (i.p.), sniffing bouts were highly synchronized with enhanced Ca<sup>2+</sup> signals, as indicated by a notable increase in fluorescence intensity (Figures 2B and 2C). This finding suggests a direct and temporally precise relationship between the activation of OVLT<sup>Glut</sup> neurons and the initiation of sniffing in response to hypertonic stimulation.

To verify whether OVLT<sup>Glut</sup> neurons are essential for the generation of thirst-driven sniffing, we performed a loss-of-function experiment using an optogenetic approach to silence these neurons. This was achieved by delivering a virus encoding eNpHR into the OVLT in Vglut2-Cre mice (Figure 2D). Initially, electrophysiological validation was conducted to confirm the effectiveness of the optogenetic inhibition. This involved monitoring spontaneous firing in fluorescently labeled OVLT<sup>Glut</sup> neurons in hypothalamic slices using a cell-attached patch-clamp configuration (Figure 2D). The average firing rate in eight neurons increased from 0.68 ± 0.20 Hz to 1.20 ± 0.30 Hz when the bath solution Na<sup>+</sup> concentration was raised from 150 mM to 160 mM. However, this effect was quickly reduced or eliminated with 589-nm illumination (30 mW, 10 Hz, light in solution), demonstrating the feasibility and effectiveness of optogenetic inhibition of OVLT<sup>Glut</sup> neurons (Figures 2E and 2F).

Thereafter, to further examine whether *in vivo* silencing OVLT<sup>Glut</sup> neurons affected the onset of sniffing in mice challenged by hypertonic solution, OVLT<sup>Glut</sup> neurons were illuminated with constant yellow light (589 nm, 10 mW). The illumination did not significantly influence the baseline breathing pattern but led to a significant reduction in sniffing episodes following injection of 2 M NaCl (i.p.) (Figures 2G and 2H). This was reflected by a reduced BF (Figures 2I and 2J), PIF (Figures 2K and 2L), and sniffing time (Figures 2M and 2N). Collectively, these results indicate that the silencing of OVLT<sup>Glut</sup> neurons results in a reduction in episodes of thirst-driven exploratory sniffing.

### Photostimulation of OVLT<sup>Glut</sup> neurons induces sniffing

To assess whether the activation of OVLT<sup>Glut</sup> neurons induced sniffing in satiated mice, an optogenetic strategy was employed.

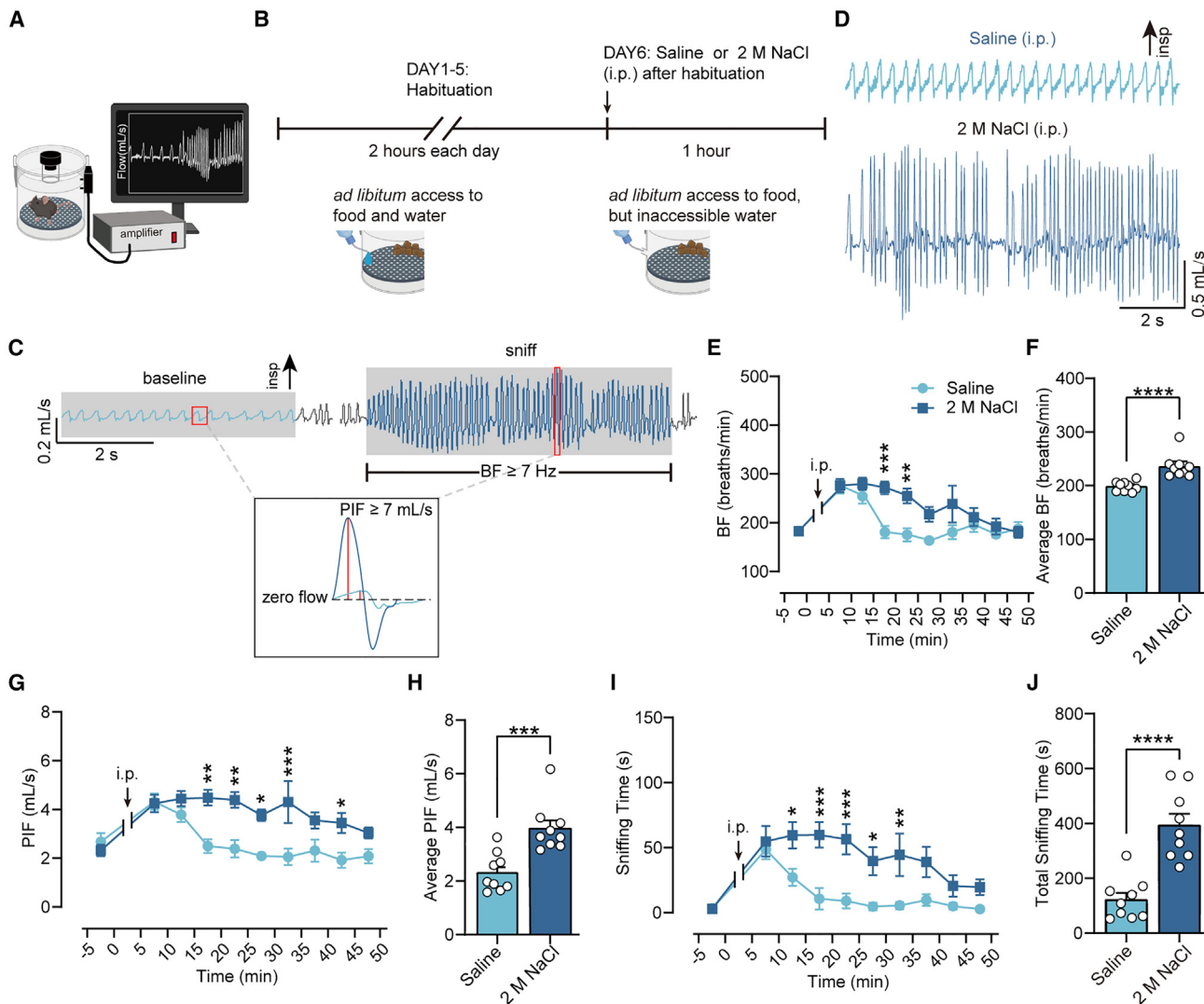


**Figure 1. Hypertonic stimulation increases sniffing episodes**

(A) Schematic of the WBP setup.

(B) Outline of the experimental procedure.

(C) Example airflow traces illustrating eupneic breathing and sniffing. The lower panel is an enlarged view combining individual eupneic and sniffing respiratory waveforms.

(D) Typical WBP recordings from C57 mice, illustrating the effects of intraperitoneal (i.p.) injections of saline and 2 M NaCl on sniffing episodes.

(E–J) Analysis of sniffing episodes under hypertonic conditions. The temporal profiles of changes in average BF (E), average PIF (G), and sniffing time (I) was measured at 5-min intervals over a 50-min period following injection of either saline or 2 M NaCl. Quantitative analysis of group data was made over the 50-min period (F, H, and J).  $n = 9$  mice for each group.  $*p < 0.05$ ,  $**p < 0.01$ ,  $***p < 0.001$ ,  $****p < 0.0001$ , as determined by two-way ANOVA with Bonferroni's multiple comparisons tests (E, G, and I), two-tailed Mann-Whitney test (F), and two-tailed unpaired t test (H and J). Details of the statistical analyses and  $p$  values of each dataset in (E)–(J) are provided in Table S1. Data are expressed as the mean  $\pm$  SEM.

See also Video S1.

Specifically, a virus encoding ChR2 was delivered into the OVLT of Vglut2-Cre mice, while a control group received a virus expressing only mCherry. The expression of ChR2 in the OVLT was confirmed using immunohistochemical detection (Figure 3A). Following habituation, programmed photostimulation of OVLT<sup>Glut</sup> neurons (10 mW, 10 Hz; laser on for 1 s, off for 3 s, over a 10-min period) rapidly elicited exploratory sniffing episodes (Figure 3B), characterized by increased BF (Figure 3C), higher PIF

(Figure 3D), and prolonged sniffing duration (Figure 3E). Consistent with these physiological changes, video analysis revealed that the proportion of exploration time (defined as the percentage of the 10-min laser-on period during which the mice exhibited head raises, circling, and standing behaviors) was significantly greater in the ChR2-injected mice compared to their counterparts (Figure 3F and Video S2). These results demonstrate that sustained photostimulation of OVLT<sup>Glut</sup> neurons is sufficient to elicit

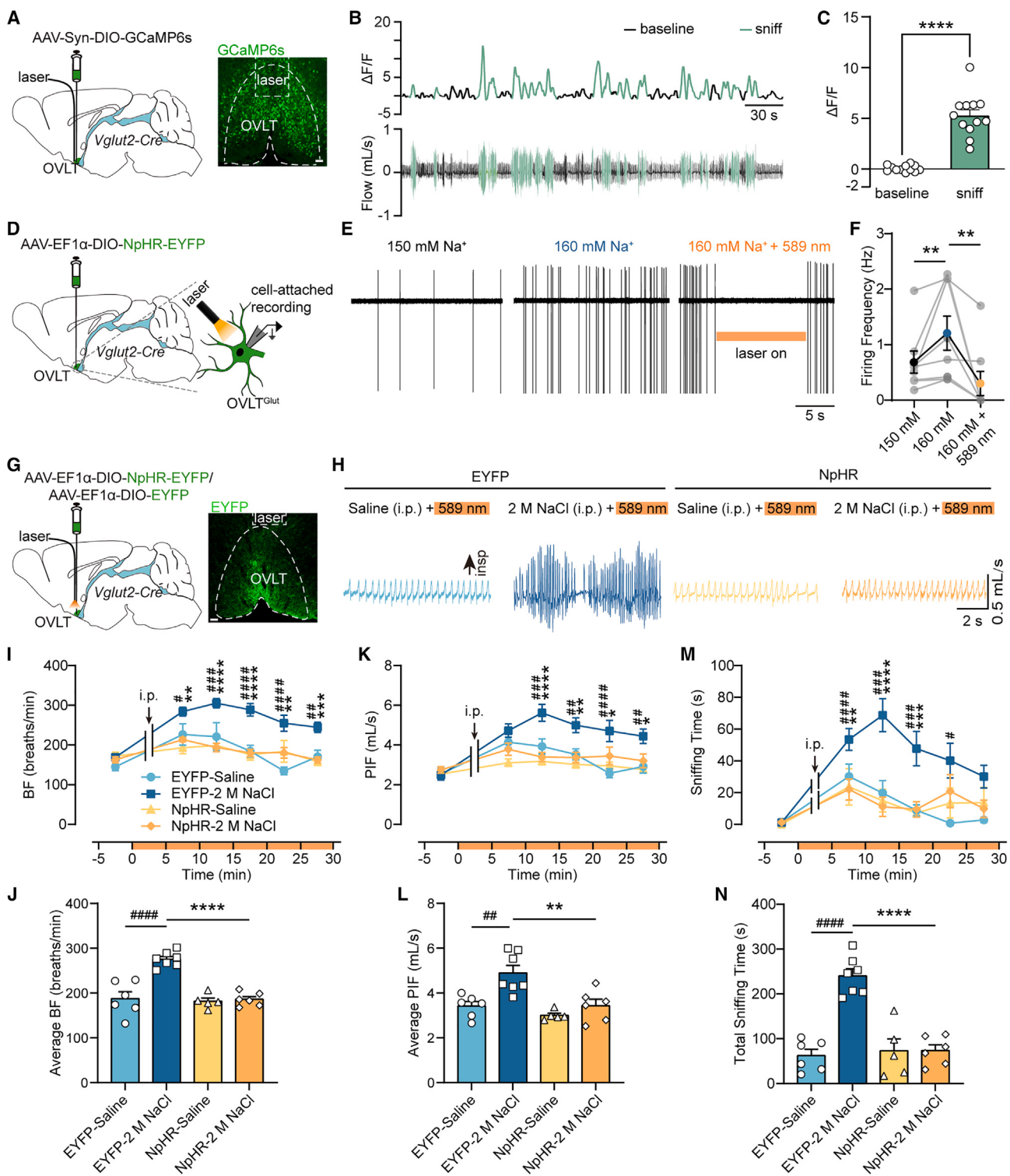


**Figure 2. Silencing of OVLT<sup>Glut</sup> neurons reduces occurrence of sniffing induced by hypertonic stimulation**

(A) Illustration of the viral injection strategy of *in vivo* Ca<sup>2+</sup> imaging (left) and immunohistochemical detection of GCaMP6s expression in the OVLT of a Vglut2-Cre mouse (right). Scale bar, 50  $\mu$ m.

(B) Example recordings showing that onset of sniffing was synchronized with elevated activation level of OVLT<sup>Glut</sup> neurons when challenged by hypertonic stimulation

(legend continued on next page)

sniffing episodes, mimicking the effects observed following i.p. injection of a hypertonic solution.

Sniffing is commonly considered as a specialized respiratory behavior, characterized by a high-frequency and high-amplitude breathing pattern.<sup>3,30</sup> Therefore, it is inferred that sniffing originates from an enhanced central respiratory drive, which is typically assessed by recording phrenic nerve discharge (PND). To address this issue, we conducted experiments via combined application of photostimulation (473 nm, 10 mW, 10 Hz, 60 s) of OVLT<sup>Glut</sup> neurons and PND recordings in anesthetized, satiated mice (Figure 3G). Optogenetic activation of OVLT<sup>Glut</sup> neurons produced a robust increase in the frequency of PND, while the amplitude remained largely unaltered (Figures 3H–3J). These results indicate that photostimulation of OVLT<sup>Glut</sup> neurons significantly enhanced central respiratory drive.

#### Photostimulation of OVLT<sup>Glut</sup> neurons projecting to the PVN elicits sniffing behaviors

To identify the circuits responsible for thirst-driven sniffing, we first analyzed the downstream brain regions targeted by OVLT<sup>Glut</sup> neurons using an anterograde neural tracing strategy. We delivered AAV-hSyn-DIO-mCherry into the OVLT of Vglut2-Cre mice (Figure S2A). Immunohistochemical analysis revealed that these neurons primarily projected to the pons, thalamus, hypothalamus, and brainstem (Figures S2B and S2C). Specifically, axonal terminals were found in the regions associated with breathing regulation, such as the PVN, locus coeruleus (LC), lateral parabrachial nucleus (LPBN), and NTS. However, very weak signals were detected in the preBötC, a core structure responsible for inspiratory rhythmogenesis (Figures S2B and S2C).

Next, we selectively photostimulated axonal terminals located in downstream targets of OVLT<sup>Glut</sup> neurons in ChR2-injected satiated mice (Figure 4A) while simultaneously monitoring PND. This approach enabled us to identify potential downstream targets of OVLT<sup>Glut</sup> neurons involved in generating sniffing behaviors. The results showed that stimulation of axonal terminals within the SFO, PVN, LH, and dorsomedial hypothalamus (DMH) significantly increased the PND frequency but not amplitude, while no similar effect was observed upon stimulation of the LPBN, LC, and NTS (Figures 4B and 4C). Given the pivotal role of the preBötC in respiratory control, we specifically explored the conse-

quences of illuminating the preBötC on PND activity but found no significant changes in PND. This outcome is consistent with our neural tracing analysis, which detected no significant signals of OVLT<sup>Glut</sup> axons within the preBötC. Our results concur with a previous study that also revealed no significant anatomical connectivity between the OVLT and the preBötC.<sup>31</sup>

Considering that the SFO and OVLT are both circumventricular organs, they may play parallel roles as central osmoreceptors, and there is a complex interplay between them through reciprocal projections.<sup>23</sup> Consequently, we have prioritized the PVN, LH, and DMH as candidate downstream targets of OVLT<sup>Glut</sup> neurons. To validate this hypothesis, we employed a similar optogenetic strategy to determine whether activation of OVLT<sup>Glut</sup> neuron axon terminals within these regions could trigger sniffing in awake Vglut2-Cre mice. Immunohistochemical analysis confirmed that ChR2-expressing axon terminals were located in the PVN (Figure 4D), LH (Figure S3A), and DMH (Figure S3E). Our results demonstrated that photostimulation of OVLT<sup>Glut</sup> neuron axon terminals within the PVN induced pronounced sniffing in satiated, freely moving ChR2-injected mice compared to control mice (Figure 4E and Video S3). This was evidenced by a remarkable increase in BF (Figure 4F), PIF (Figure 4G), total duration of sniffing (laser off vs. laser on,  $3.9 \pm 2.9$  vs.  $178.8 \pm 31.2$  s, Figure 4H), and the proportion of exploration time (Figure 4I). However, photostimulation of OVLT<sup>Glut</sup> axon terminals in the LH and DMH did not significantly increase sniffing episodes (sniffing time:  $5.6 \pm 4.7$  vs.  $17.8 \pm 7.0$  s for LH, Figures S3B–S3D;  $0.6 \pm 0.6$  vs.  $28.0 \pm 17.5$  s for DMH; Figures S3F–S3H; laser off vs. laser on). Therefore, we suggest that the PVN plays a pronounced role in mediating sniffing induced by the activation of OVLT<sup>Glut</sup> neurons.

#### Synaptic connections between OVLT<sup>Glut</sup> neurons and PVN neurons projecting to the preBötC

To investigate whether OVLT<sup>Glut</sup> neurons establish synaptic inputs to preBötC-projecting PVN neurons, we employed a triple-viral-vector approach in Vglut2-Cre mice. Three viral vectors, namely AAV-CAG-DIO-mWGA-Flpo, AAV-hSyn-fDIO-EYFP, and AAVretro-hSyn-mCherry, were injected into the OVLT, PVN, and preBötC, respectively (Figure 5A). The vector encoding the wheat germ agglutinin (WGA), an anterograde transsynaptic tracer, was used to target the postsynaptic

(C) Quantitative analysis of  $\text{Ca}^{2+}$  signals, indicated by fluorescence intensity, during baseline and sniffing.  $\Delta F/F (\%)$  indicates the change in fluorescence normalized to background fluorescence. ( $n = 4$  mice, three sessions per mouse; \*\*\* $p < 0.0001$ , two-tailed unpaired t test with Welch's correction).

(D) Schematic of the optogenetic strategy and cell-attached patch-clamp recordings from EYFP-expressing OVLT<sup>Glut</sup> neurons in brain slices from Vglut2-Cre mice.

(E) Typical traces showing changes in spontaneous firing of an EYFP-expressing neuron during bath application of 150 mM  $\text{Na}^+$  (left), 160 mM  $\text{Na}^+$  (middle), and 160 mM  $\text{Na}^+$  in conjunction with yellow laser illumination (589 nm, 30 mW, 10 Hz) (right), respectively.

(F) Quantification of pooled electrophysiological data. ( $n = 8$  cells from three mice; \*\* $p < 0.01$ , two-sided Wilcoxon's signed-rank test).

(G) Left: diagram of the viral injection strategy of optogenetics. Right: immunohistochemical validation of NpHR expression (green) in the OVLT<sup>Glut</sup> neurons. Scale bar, 50  $\mu\text{m}$ .

(H) Typical airflow traces in Vglut2-Cre mice recorded after i.p. injections of saline or 2 M NaCl, followed by 589-nm laser illumination. These recordings were from mice injected with a virus encoding NpHR-EYFP or EYFP only.

(I–N) (I, K, and M) Effect of illumination on BF, PIF, and sniffing time in NpHR-EYFP and EYFP groups following i.p. saline or 2 M NaCl injections (EYFP-saline:  $n = 6$  mice; EYFP-2 M NaCl:  $n = 7$  mice; NpHR-saline:  $n = 5$  mice; NpHR-2 M NaCl:  $n = 6$  mice). \* $p < 0.05$ , \*\* $p < 0.01$ , \*\*\* $p < 0.001$  (NpHR-2 M NaCl vs. EYFP-2 M NaCl); # $p < 0.05$ , ## $p < 0.01$ , ### $p < 0.001$  (EYFP-2 M NaCl vs. EYFP-saline); two-way ANOVA with Tukey's multiple comparisons tests. (J, L, and N) Quantification of average BF, PIF, and total sniffing time over a 30-min period. One-way ANOVA with Tukey's multiple comparisons tests.

Details of the statistical analyses in (C), (F), and (I)–(N) are provided in Table S1. Data are expressed as the mean  $\pm$  SEM. See also Figure S1.

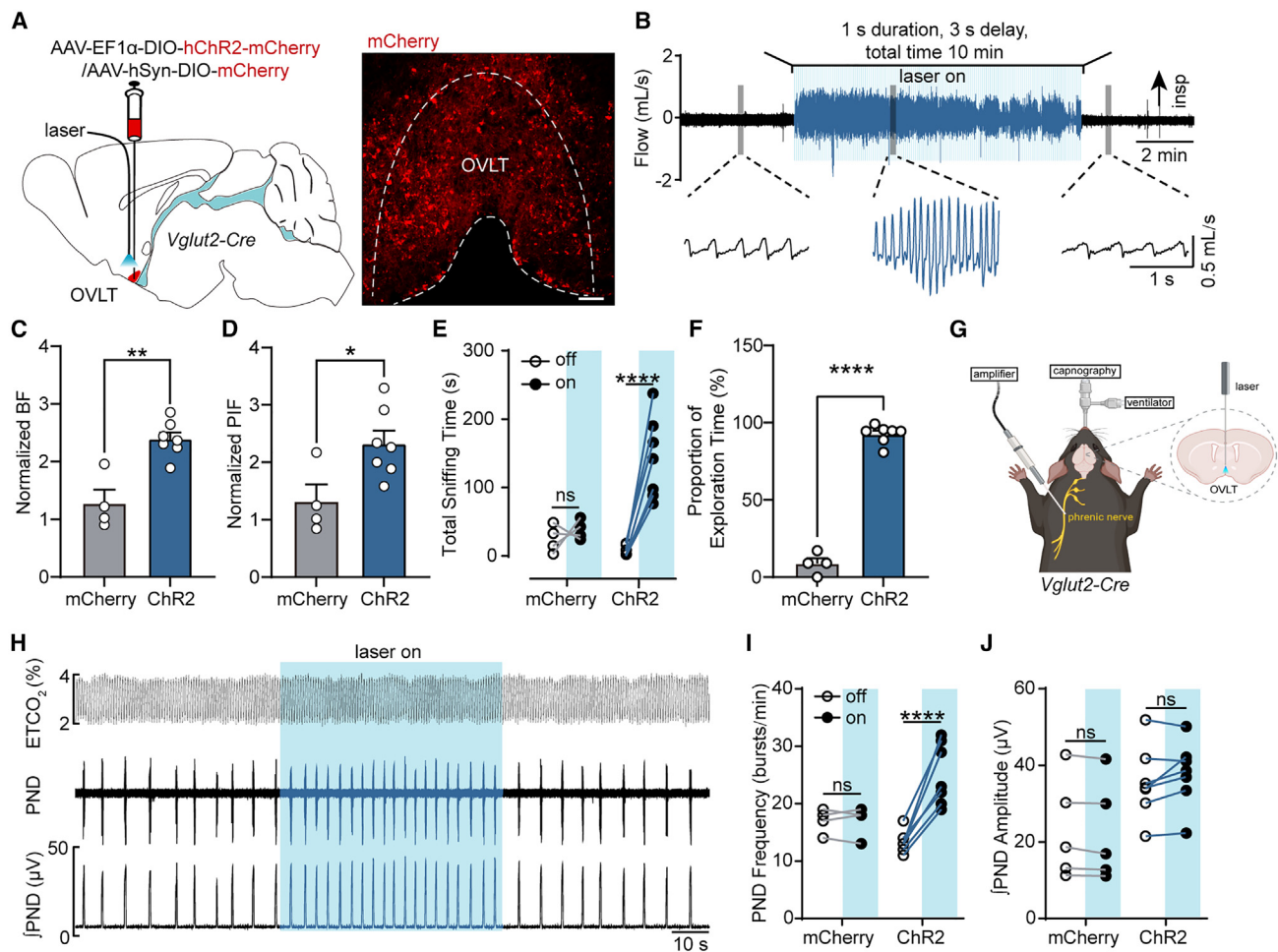


**Figure 3. Photostimulation of OVLT<sup>Glut</sup> neurons increases sniffing and PND frequency**

(A) Left: schematic of the optogenetic strategy. Right: immunohistochemical validation of ChR2 expression in the OVLT<sup>Glut</sup> neurons. Scale bar, 50  $\mu$ m.

(B) Typical airflow traces (top) indicating that programmed photostimulation (10 mW, 10 Hz) of OVLT<sup>Glut</sup> neurons over a 10-min period significantly increased sniffing episodes. Enlarged views from the top regions are shown in the bottom traces.

(C–E) Quantification of normalized BF, PIF, and total sniffing time over a 10-min period ( $n = 4$  mice in mCherry group,  $n = 7$  mice in ChR2 group).

(F) Proportion of exploration time from video analysis during 10 min of laser illumination in the mCherry ( $n = 4$  mice) and ChR2 ( $n = 7$  mice) groups.

(G) Illustration of phrenic nerve discharge (PND) recordings in Vglut2-Cre mice with injections of the virus encoding ChR2 in the OVLT<sup>Glut</sup>.

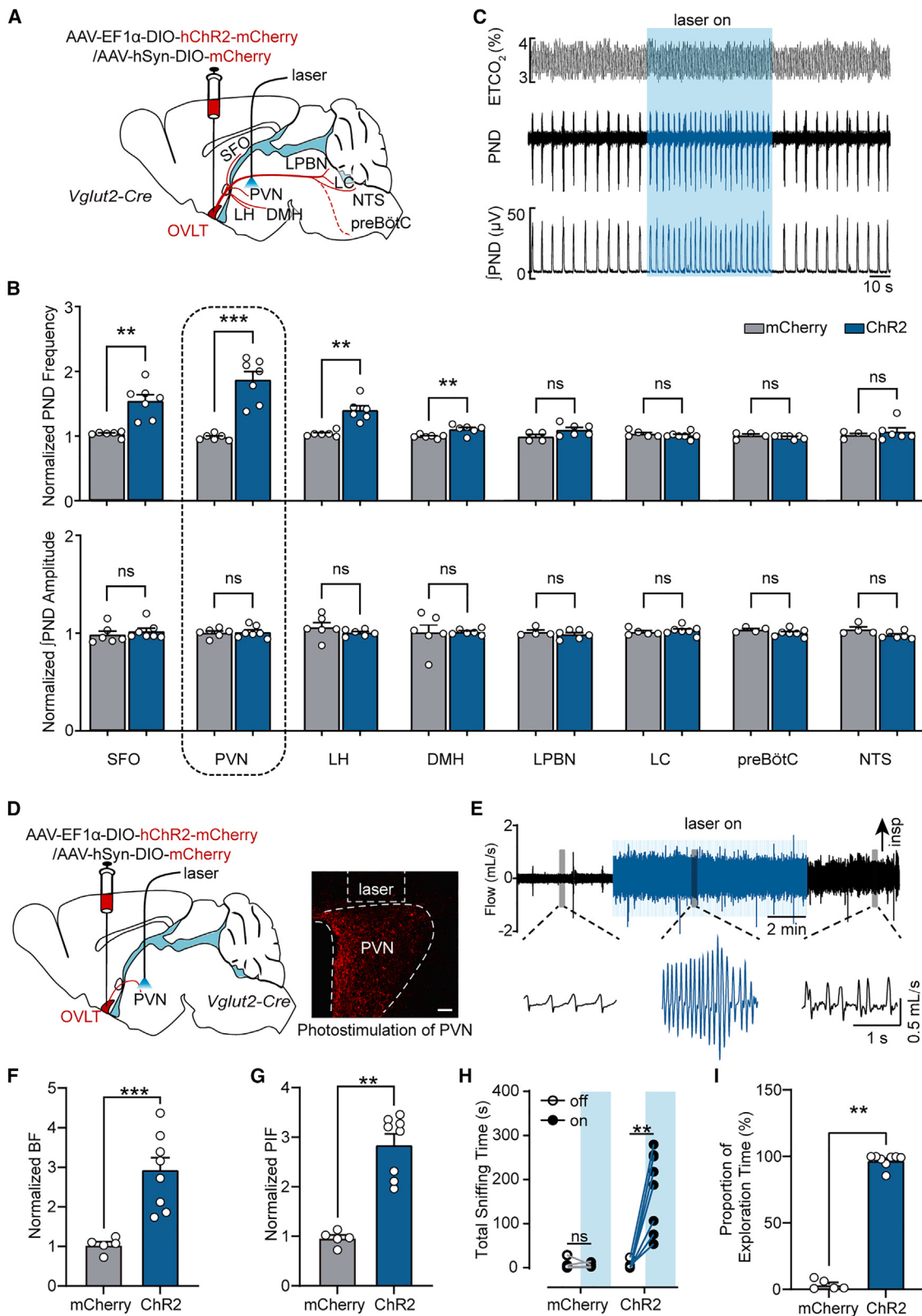
(H) Representative traces of photostimulation effect on PND activity. Top: ETCO<sub>2</sub>; middle: raw waveforms of PND; bottom: PND integration derived from rectification and smoothing (time constant, 0.05 s).

(I and J) Quantitative analysis of PND frequency and amplitude in mice injected with ChR2 ( $n = 7$  mice) vs. mCherry only ( $n = 5$  mice).

\* $p < 0.05$ , \*\* $p < 0.01$ , \*\*\* $p < 0.0001$ , as determined by two-tailed unpaired t test (C, D, and F) and two-tailed paired t test (E, I, and J). Details of the statistical analysis in (C)–(F), (I), and (J) are provided in Table S1. Data represent the mean  $\pm$  SEM. ns, not significant. See also Video S2.

neurons of OVLT<sup>Glut</sup> neurons, as previously reported.<sup>32</sup> Using this neural tracing approach, we were able to identify PVN neurons that receive inputs from OVLT<sup>Glut</sup> neurons and concurrently project to the preBötC. These neurons were marked by the co-expression of mCherry and EYFP. As illustrated in Figure 5B, we identified EYFP<sup>+</sup> neurons in the PVN that were innervated by OVLT<sup>Glut</sup> neurons, mCherry<sup>+</sup> neurons in the PVN that projected to the preBötC, and EYFP<sup>+</sup>mCherry<sup>+</sup> neurons both targeted by OVLT<sup>Glut</sup> neurons and that projected to the preBötC. Quantitative analysis revealed that mCherry<sup>+</sup>EYFP<sup>+</sup> neurons accounted for 7%  $\pm$  1% of the total EYFP<sup>+</sup> neurons and 21%  $\pm$  3% of the total mCherry<sup>+</sup> neurons (Figure 5C).

To elucidate the synaptic contact mode between PVN-projecting OVLT<sup>Glut</sup> neurons and preBötC-projecting PVN neurons, AAVretro-hSyn-EYFP was injected into the preBötC to label PVN neurons projecting to the preBötC, while AAV-EF1 $\alpha$ -DIO-hChR2-mCherry was injected into the OVLT to enable the expression of ChR2 in OVLT<sup>Glut</sup> neurons (Figure 5D). Employing a whole-cell patch-clamp mode, we monitored changes in excitatory postsynaptic currents (EPSCs) in EYFP-expressing PVN neurons in brain slices in response to photostimulation of ChR2-expressing OVLT<sup>Glut</sup> axon terminals in the PVN (Figure 5D). Our results showed that a subset of EYFP<sup>+</sup> neurons in the PVN (12 out of 26, 46%) produced no evoked EPSCs upon photostimulation,



(legend on next page)

whereas the remaining neurons (14 out of 26, 54%) generated EPSCs (Figures 5E and 5F).

Furthermore, to determine whether the EPSCs were evoked through monosynaptic connections, pharmacological experiments were performed using tetrodotoxin (TTX), 4-aminopyridine (4-AP), and 6-cyano-7-nitroquinoxaline-2,3-dione (CNQX). In 9 out of 26 (35%) neurons, combined bath application of TTX and 4-AP reversibly abolished the photostimulation-evoked EPSCs in favor of a polysynaptic mechanism (Figures 5G and 5H). In 5 out of 26 (19%) neurons, the combined application of TTX and 4-AP did not significantly affect the amplitude of evoked EPSCs, while these evoked EPSCs were eliminated by CNQX administration (Figures 5I and 5J). This indicates that these evoked EPSCs were generated through monosynaptic connections established by OVLT<sup>Glut</sup> neurons projecting to the PVN and PVN neurons projecting to the preBötC, and meanwhile this excitatory synaptic transmission was mediated by glutamate. Collectively, our data suggest that OVLT<sup>Glut</sup> neurons regulate the activity of PVN neurons projecting to the preBötC through either monosynaptic or polysynaptic mechanisms or a combination of both.

Furthermore, although it remains uncertain whether stimulation of PVN neurons projecting to the preBötC directly activates breathing, it has been shown that these neurons play a role in the control of respiration.<sup>33</sup> By injecting the AAVretro-EF1 $\alpha$ -hChR2-EYFP virus into the preBötC in C57BL/6J mice, we identified the distribution of ChR2-EYFP-expressing neurons in the PVN (Figure S4A). Photostimulation of these neurons resulted in a frequency-dependent increase in PND frequency but not amplitude (Figures S4B–S4D), indicating that PVN neurons make a significant contribution to respiratory motor output. This result aligns with the effects produced through the photostimulation of OVLT<sup>Glut</sup> neurons (Figures 3H–3J). Altogether, these results support the concept that the stimulation of OVLT<sup>Glut</sup> neurons induces sniffing behaviors through activation of the PVN-preBötC pathway.

#### Ablation of PVN neurons projecting to the preBötC inhibited sniffing induced by activation of OVLT<sup>Glut</sup> neurons and prolonged drinking latency

To further ascertain whether the PVN-preBötC pathway mediated the occurrence of sniffing evoked by activation of OVLT<sup>Glut</sup> neurons, loss-of-function experiments were conducted by delivery

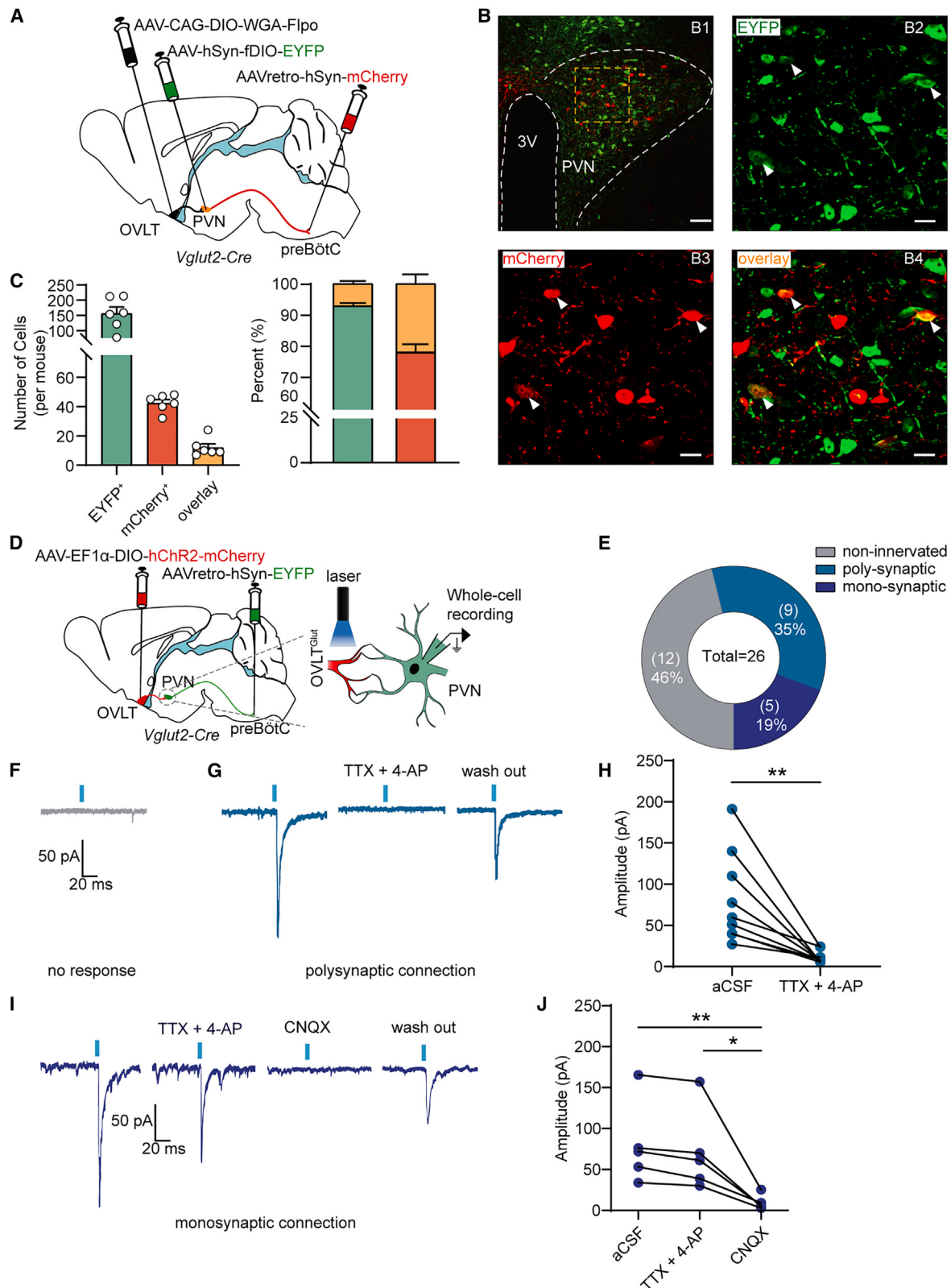
of a virus encoding caspase-3 (Casp3) into the PVN from Vglut2-Cre mice to induce apoptosis of PVN neurons projecting to the preBötC. To facilitate the expression of the ChR2 tagged with the mCherry fluorescent marker in the OVLT<sup>Glut</sup> neurons, the AAV-EF1 $\alpha$ -DIO-hChR2-mCherry viral vector was injected into the OVLT. Ten days post injection, we proceeded with the injections of the AAV-EF1 $\alpha$ -fDIO-taCasp3 into the PVN and the AAVretro-hSyn-Flpo-EYFP viral vector into the preBötC (Figures 6A and 6B). This sequential injection procedure enabled us to stimulate the OVLT<sup>Glut</sup> axon terminals within the PVN and monitor sniffing episodes with or without ablation of PVN neurons projecting to the preBötC.

Subsequently, immunohistochemical detection revealed a high density of OVLT<sup>Glut</sup> neuron axon terminals expressing mCherry (red) in the PVN (Figure 6C). The EYFP-expressing PVN neurons projecting to the preBötC (green) were identified in the mice that received the injection of control virus lacking Casp3 (AAVretro-hSyn-Flpo-EYFP) into the preBötC, while very few such neurons were detected in mice injected with the virus encoding Casp3, confirming the feasibility of the viral lesion technique (Figure 6C). In a satiated state, compared with the control group, loss of PVN neurons projecting to the preBötC significantly attenuated the sniffing bouts upon photostimulation of OVLT<sup>Glut</sup> neuronal axon terminals in the PVN (Figure 6D). This was reflected by a remarkable decrease in BF (Figure 6E), PIF (Figure 6F), and sniffing time (Figure 6G). In contrast, video analysis revealed no significant difference in the proportion of exploration time between the control and taCasp3 groups (Figure 6H). These findings jointly demonstrate that the OVLT-PVN-preBötC circuit primarily mediates sniffing behavior but have no significant impact on exploratory time. Next, we tested whether the PVN-preBötC circuit contributes to regulation of thirst-driven sniffing. The procedure involved ablation of PVN neurons projecting to the preBötC (Figure 6I) followed by application of hypertonic stimulation (Figure 6J). Our results demonstrate that the increased sniffing time induced by 2 M NaCl (i.p.) injection was significantly reduced in mice with loss of PVN neurons projecting to the preBötC as compared to control mice (Figures 6K and 6L).

To assess whether lesioning the PVN-preBötC pathway reduced exploratory sniffing and thereby affected water-seeking and water-drinking behaviors, we utilized a chamber equipped with a camera to concurrently monitor photostimulation and

**Figure 4. Photostimulation of the OVLT<sup>Glut</sup>-PVN pathway induces sniffing**

- (A) Illustration of the optogenetic strategy. Solid lines: nuclei with an axonal distribution. Dotted lines: nucleus without an axonal distribution.
  - (B) Normalized PND frequency (top) and amplitude (bottom) in mCherry and ChR2 groups before and after photostimulation of OVLT<sup>Glut</sup> axon terminals in brain regions (SFO, PVN, LH, DMH, LPBN, LC, preBötC and NTS) with sample sizes (*n*) ranging from 4 to 7 mice per group. \*\**p* < 0.01, \*\*\**p* < 0.001, two-tailed unpaired *t* test.
  - (C) Representative PND traces showing that photostimulation of axon terminals of OVLT<sup>Glut</sup> neurons in the PVN significantly increased PND frequency.
  - (D) Left: schematic of photostimulation. Right: immunohistochemical verification of axons of OVLT<sup>Glut</sup> neurons in the PVN. Scale bar, 50  $\mu$ m.
  - (E) Example recordings of airflow during photostimulation of axon terminals of OVLT<sup>Glut</sup> neurons in the PVN from ChR2-injected mice.
  - (F–H) Quantification of normalized BF and PIF, as well as total sniffing time in mCherry and ChR2 groups (*n* = 5 mice for mCherry, *n* = 8 mice for ChR2). Normalized BF: ChR2 vs. mCherry, *p* = 0.0007, two-tailed unpaired *t* test with Welch's correction; normalized PIF: ChR2 vs. mCherry, *p* = 0.0016, two-tailed Mann Whitney test; total sniffing time: laser on vs. laser off, *p* > 0.9999 for mCherry, *p* = 0.0078 for ChR2, two-sided Wilcoxon's signed-rank test for both.
  - (I) Proportion of exploration time based on video recording analysis during 10 min of laser illumination in the mCherry (*n* = 5 mice) and ChR2 (*n* = 8 mice) groups. *p* = 0.0016, two-tailed Mann Whitney test.
- SFO, subfornical organ; PVN, paraventricular nucleus; LH, lateral hypothalamus; DMH, dorsomedial hypothalamic nucleus; LPBN, lateral parabrachial nucleus; LC, locus coeruleus; preBötC, preBötzingen complex; NTS, nucleus tractus solitarius. Details of the statistical analysis in (B) and (F–I) are shown in Table S1. Data represent the mean  $\pm$  SEM. ns, not significant; \*\**p* < 0.01, \*\*\**p* < 0.001. See also Figures S2 and S3; Video S3.



(legend on next page)

drinking behaviors in satiated mice (Figure 6M). The drinking latency was defined as the interval from the onset of laser stimulation to the initiation of drinking from the lick port. Mice were acclimated in the chamber for 1 h without access to water. Subsequently, illumination (10 mW, 10 Hz; laser on for 1 s, off for 3 s, over 10 min) was applied to stimulate the axonal terminals of OVLT<sup>Glut</sup> neurons in the PVN while providing *ad libitum* access to water. Upon photostimulation, the control mice quickly located the water spout and began drinking. However, mice with PVN-preBötC ablation required a relatively longer time to locate the water spout (Figure 6N). Interestingly, once these mice located the spout and began drinking, their total drinking time (Figures 6O and 6P) and water consumption (Figure 6Q) was not statistically significant compared to the control group. However, the proportion of drinking time in the first minute relative to the total drinking time over the 10-min photostimulation period was significantly different between the control group and the taCasp3 group (Figure 6R). This difference may be attributable to the extended latency to drink in the ablation-group mice. Collectively, these data indicate that ablation of pre-BötC-projecting PVN neurons significantly reduces thirst-driven sniffing and increases latency to drinking in response to activation of OVLT<sup>Glut</sup> neurons, further confirming the critical role of the OVLT<sup>Glut</sup>-PVN-preBötC circuit in the regulation of thirst-driven sniffing.

## DISCUSSION

Thirst represents a fundamental physiological demand that prompts exploratory behaviors aimed at quenching this need. In response to this innate drive, biological evolution has facilitated the development of complex exploratory behaviors, such as sniffing, that enable efficient exploration and information gathering to satisfy this internal demand.<sup>18</sup> In the present study, we demonstrate that hypertonic stimulation robustly increases sniffing and that optogenetic inhibition of OVLT<sup>Glut</sup> neurons effectively reduces this behavior. Moreover, stimulation of OVLT<sup>Glut</sup> neurons elicits pronounced sniffing, characterized by increased BF and PIF. Furthermore, activation of OVLT<sup>Glut</sup> neuron axons projecting to the PVN induces sniffing. In contrast, genetic ablation of PVN

neurons projecting to the preBötC significantly diminishes the onset of sniffing. Additionally, lesions of PVN neurons projecting to the preBötC prolong the drinking latency. These findings collectively suggest that the OVLT<sup>Glut</sup>-PVN-preBötC circuit plays a crucial role in the regulation of thirst-driven sniffing and the efficiency of water-seeking behaviors.

### OVLT<sup>Glut</sup> neurons contribute to induction of thirst-driven sniffing

Because they lack high-acuity foveal vision, rodents are thought to rely heavily on nonvisual information, especially tactile and olfactory information.<sup>34</sup> Sniffing is a complex behavior whereby animals gather olfactory information by taking deep breaths through their nose.<sup>3</sup> It entails multiple aspects such as olfaction, motor output, respiration, motivation, reward, and arousal.<sup>7,35</sup> Animals also respond to their environment during sniffing, such as experiencing reward when detecting food scents, feeling motivated to search for water or escape danger, and becoming more alert with warning scents.<sup>5,6,34,36</sup> Sniffing is also a specific respiratory pattern, commonly characterized by high BF and PIF.<sup>3</sup> Consistent with this concept, the present study indicates that hypertonic stimulation remarkably increases sniffing episodes in awake mice, with increased BF and PIF.

Based on accumulated evidence and the present data, we propose that hypertonic stimulation-induced sniffing is mediated by OVLT neurons. Initially, hypertonic stimulation elevated the activation level of OVLT neurons. It has been found that 70% of the neurons in the OVLT are glutamatergic, while 30% are GABAergic.<sup>20</sup> Moreover, a previous *in vivo* study using single-unit recordings showed that 72% of OVLT neurons exhibit concentration-dependent increases in neuronal discharge when challenged with infusion of hypertonic NaCl.<sup>24</sup> These studies suggest that the majority of thirst-promoting neurons in the OVLT are glutamatergic, although there are reports suggesting that a subset of GABAergic neurons may also be intrinsically osmo-sodium sensitive.<sup>37</sup> Our immunohistochemical analysis extends these investigations by demonstrating that 79% of hypertonic-solution-activated OVLT neurons are glutamatergic. Furthermore, in the presence of hypertonic stimulation, sniffing bouts were highly synchronized with activated OVLT<sup>Glut</sup> neurons, as indicated by

**Figure 5. Anatomical and functional connections between OVLT<sup>Glut</sup> neurons projecting to the PVN and PVN neurons projecting to the preBötC**

- (A) Schematic of the neural tracing strategy by delivering an anterograde virus encoding wheat germ agglutinin (WGA) into the OVLT.
- (B) Typical photomicrographs showing postsynaptic neurons of OVLT<sup>Glut</sup> neurons in the PVN (green, EYFP), PVN neurons projecting to the preBötC (red, mCherry) and OVLT<sup>Glut</sup>-innervated PVN neurons projecting to the preBötC (yellow, overlay). Images B2–B4 are enlarged views as indicated by the yellow square in B1. Scale bars, 50 μm (B1) and 20 μm (B2–B4).
- (C) Left: quantification of the number of EYFP<sup>+</sup> neurons ( $n = 156 \pm 22$  cells), mCherry<sup>+</sup> neurons ( $n = 42 \pm 2$  cells), and their co-targets ( $n = 12 \pm 3$  cells). Right: co-targeted neurons account for 7% ± 1% of the total EYFP<sup>+</sup> neurons and 21% ± 3% of the mCherry<sup>+</sup> neurons.  $n = 6$  mice.
- (D) Schematic of the viral injection strategy and whole-cell patch-clamp recordings of excitatory postsynaptic currents (EPSCs) in PVN neurons projecting to the preBötC in brain slices. The EPSCs were evoked by photostimulation of OVLT<sup>Glut</sup> neuronal axons in the PVN.
- (E) Classification of PVN neurons projecting to the preBötC into three subgroups based on their responses to photostimulation of OVLT<sup>Glut</sup> neuron terminals: unresponsive neurons (gray, 46%); neurons with polysynaptic connections (blue, 35%); neurons with monosynaptic connections (purple, 19%).  $n = 26$  neurons from five mice.
- (F) Unresponsive neurons showed no light-evoked EPSC.
- (G and H) Neurons with polysynaptic connections exhibited light-evoked EPSCs that were blocked by TTX + 4-AP ( $n = 9$  cells,  $p = 0.0039$ , two-sided Wilcoxon's signed-rank test).
- (I and J) Neurons with monosynaptic connections displayed light-evoked EPSCs that were not blocked by TTX + 4-AP but were abolished by CNQX ( $n = 5$  cells; CNQX vs. artificial cerebrospinal fluid [aCSF],  $p = 0.0048$ ; CNQX vs. TTX + 4-AP,  $p = 0.0010$ , one-way repeated-measures ANOVA).
- Details of the statistical analyses in (H) and (J) are shown in Table S1. Data are presented as mean ± SEM. \* $p < 0.05$ , \*\* $p < 0.01$ . See also Figure S4.

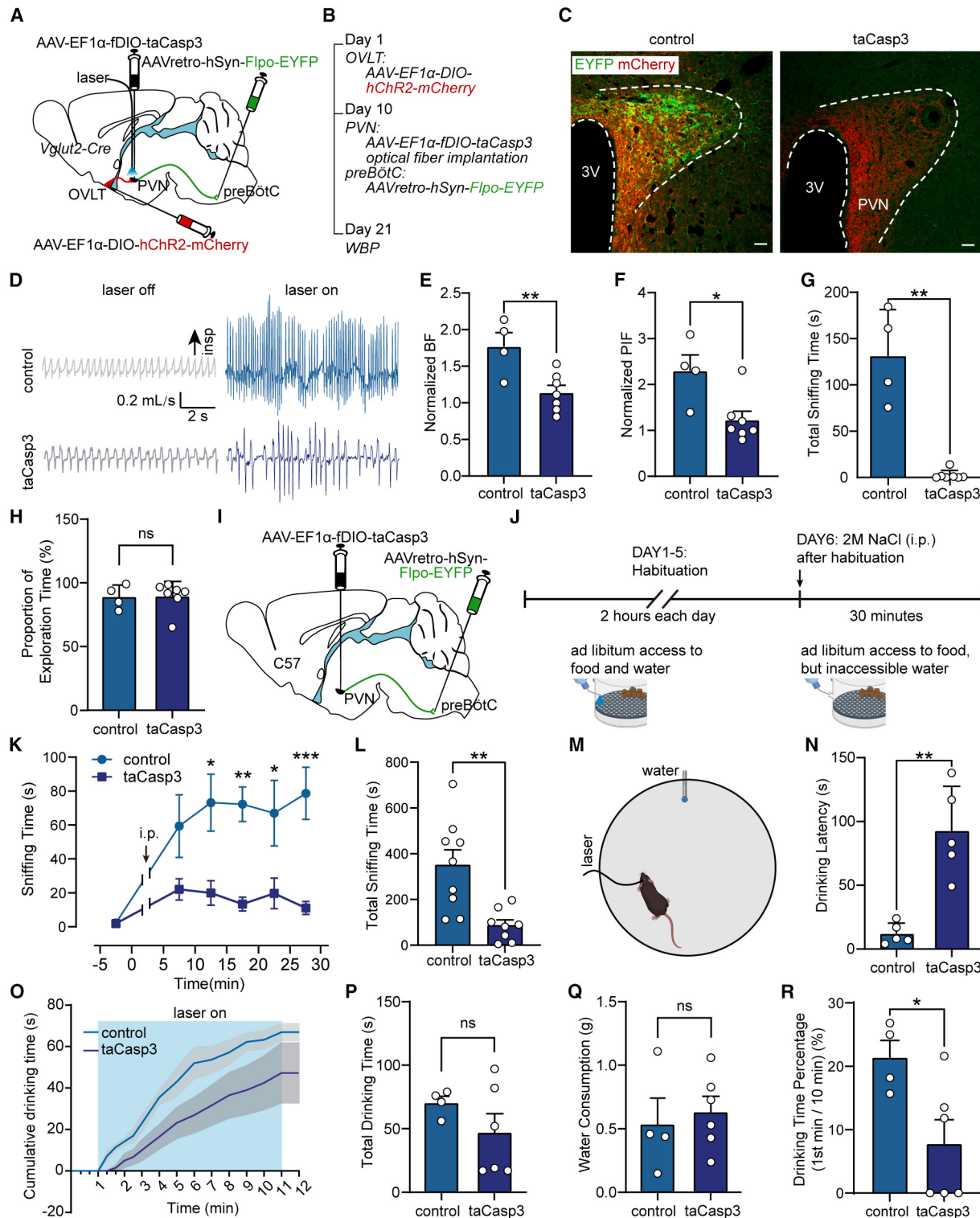


**Figure 6. Disruption of the OVLT<sup>Glut</sup>-PVN-preBötC pathway reduces sniffing episodes and prolongs the drinking latency**

(A) Schematic of the genetic ablation strategy involving bilateral injections of a virus encoding caspase-3 (taCasp3) into the PVN of Vglut2-Cre mice.

(B) Illustration of the experimental procedure.

(C) Immunohistochemical validation showing the loss of EYFP-expressing PVN neurons projecting to the preBötC in the taCasp3-injected mice (right image), whereas such neurons were present in the control group injected with a virus lacking taCasp3 (left image). Scale bars, 20  $\mu$ m.

(legend continued on next page)

enhanced  $\text{Ca}^{2+}$  signal. Additionally, optogenetic inhibition of OVLT<sup>Glut</sup> neurons significantly diminished hypertonic stimulation-elicited sniffing behaviors. Thereby, these findings underscore the considerable contribution of OVLT<sup>Glut</sup> neurons to the regulation of sniffing.

Previous studies have demonstrated that both OVLT and SFO detected various thirst-driving signals, such as angiotensin II in the blood, high  $[\text{Na}^+]$  levels, or hypertonicity in the body fluids, which were subsequently integrated in the MnPO to drive thirst.<sup>38</sup> Our findings corroborate this view, indicating that i.p. injection of hypertonic saline upregulates Fos expression in the OVLT, SFO, and MnPO. Our study primarily focuses on the role of the OVLT in thirst-driven sniffing behavior. Nevertheless, we do not exclude the possibility that the SFO and MnPO may also play a role in this process, given that these regions are extensively and reciprocally interconnected. Accumulated evidence has shown that the activity of dehydration-activated MnPO neurons establishes a scalable, persistent, and aversive internal state that dynamically coordinates thirst-motivated behavior.<sup>38</sup> Although SFO neurons display intrinsic osmosensitivity,<sup>20</sup> lesions of the SFO fail to prevent water intake induced by systemic hypertonicity.<sup>39,40</sup> Thus, osmotic thirst might not be triggered by activating SFO neurons in such conditions. Conversely, lesions encompassing the OVLT and MnPO caused adipsia<sup>41</sup> and blocked water intake induced by a hyperosmotic stimulus.<sup>21,42</sup> The OVLT is a circumventricular organ (whereas MnPO is not), which makes the OVLT a potential osmoreceptor region responsible for the control of thirst. Indeed, functional MRI studies in humans have shown that the ventral portion of the lamina terminalis, which encloses the OVLT, is activated in response to systemic hyperosmotic stimuli.<sup>43,44</sup> In addition, there are studies reporting that the water intake mediated by SFO is achieved by sending axonal projections to the OVLT,<sup>28,29</sup> although the involvement of the SFO-MnPO pathway cannot be entirely ruled out.<sup>45,46</sup>

Our findings demonstrate that photostimulation of OVLT<sup>Glut</sup> neurons vigorously triggered sniffing, an effect similar to that induced by hypertonic stimulation. To further consolidate our observations, we examined the effect of photostimulation of OVLT<sup>Glut</sup> neurons on central respiratory drive in anesthetized

mice. Given that sniffing is a specialized respiratory behavior, the onset of sniffing must be accompanied by enhanced central respiratory drive. The PND pattern has been used to assess fictive sniffs in an olfactory bulb-brainstem preparation.<sup>47</sup> Additionally, sniffing is associated with an increased rate of bursts in preBötC neurons.<sup>5</sup> In the present study, rapid stimulation of OVLT<sup>Glut</sup> neurons significantly increased PND frequency, suggesting that an enhanced central respiratory drive is linked to the occurrence of sniffing. In short, these findings collectively demonstrate that activation of OVLT<sup>Glut</sup> neurons plays a crucial role in the regulation of thirst-driven sniffing.

### Activation of the PVN-preBötC pathway by the OVLT<sup>Glut</sup> neurons: Circuit mechanisms

Although the ventrolateral medulla contributes to the regulation of sniffing,<sup>12</sup> the circuit mechanisms underlying thirst-associated sniffing remain obscure. Initially, our neural tracing data reveal that the axonal terminals of OVLT<sup>Glut</sup> neurons are widely distributed across the thalamus, hypothalamus, midbrain, and hindbrain. The projection of OVLT<sup>Glut</sup> neurons to the LH, medial habenular nucleus, paraventricular thalamic nucleus, and xiphoid thalamic nucleus in the thalamus may be involved in regulating negatively motivated behaviors, as these nuclei exhibit increased activity upon the onset of licking and reward delivery.<sup>18,48</sup> The hypothalamus is closely associated with motivated behaviors required for survival and reproduction.<sup>49</sup> Studies have shown that the activation of the LH elicits exploratory behaviors as well as high-frequency sniffing,<sup>17</sup> and the stimulation of the SFO neurons causes water-seeking behavior.<sup>48</sup> In line with these data, our findings reveal that OVLT<sup>Glut</sup> neuronal axons project to both the LH and SFO regions. The axons of OVLT<sup>Glut</sup> neurons were densely detected in the PVN, DMH, and the arcuate nucleus in the hypothalamus. This close association may be linked to the homeostatic mechanisms that regulate water and food intake<sup>50,51</sup> and breathing.<sup>52</sup> Axons of OVLT<sup>Glut</sup> neurons innervate the LC, LPBN, ventral tegmental area, dorsal raphe nucleus, and periaqueductal gray, which are likely involved in integrating functions related to arousal, appetite, reward, and goal-directed behaviors.<sup>53–57</sup> Importantly, OVLT<sup>Glut</sup> neurons have synaptic

(D) Example traces showing that the ablation of PVN neurons projecting to the preBötC significantly diminished sniffing behaviors in the taCasp3-injected mice relative to control mice upon photostimulation of OVLT<sup>Glut</sup> neuronal axons in the PVN.

(E–G) Quantitative analysis of normalized BF, PIF, and total sniffing time in control ( $n = 4$  mice) and taCasp3 ( $n = 7$  mice) groups (normalized BF:  $p = 0.0082$ , two-tailed unpaired t test; normalized PIF:  $p = 0.0242$ , two-tailed Mann-Whitney test; total sniffing time:  $p = 0.0061$ , two-tailed Mann-Whitney test).

(H) The proportion of exploration time based on video analysis ( $n = 4$  for control and  $n = 7$  for taCasp3,  $p = 0.9273$ , two-tailed Mann-Whitney test).

(I) Schematic of the genetic ablation strategy.

(J) Outline of the experimental procedure.

(K) Temporal profiles of changes in sniffing time following injection of 2 M NaCl in the control and taCasp3 groups ( $n = 9$  mice for control,  $n = 8$  mice for taCasp3; two-way ANOVA with Bonferroni's multiple comparisons test; \* $p < 0.05$ , \*\* $p < 0.01$ , \*\*\* $p < 0.001$ ).

(L) The total sniffing time from the 5th to the 30th min following injection of 2 M NaCl ( $n = 9$  mice for control,  $n = 8$  mice for taCasp3,  $p = 0.0038$ , two-tailed unpaired t test).

(M) Schematic of the measurement of latency to drinking.

(N) Quantification of drinking latency in the control and taCasp3 groups during photostimulation. ( $n = 5$  mice for control,  $n = 5$  mice for taCasp3,  $p = 0.0060$ , two-tailed unpaired t test with Welch's correction).

(O–Q) Cumulative drinking time, total drinking time, and water consumption during photostimulation in the control and taCasp3 groups ( $n = 4$  mice for control,  $n = 6$  mice for taCasp3; total drinking time:  $p = 0.2483$ , two-tailed unpaired t test; water consumption:  $p = 0.6727$ , two-tailed unpaired t test).

(R) The proportion of drinking time in the first minute relative to the total drinking time over a 10-min period ( $n = 4$  mice for control,  $n = 6$  mice for taCasp3,  $p = 0.0293$ , two-tailed unpaired t test).

Details of the statistical analyses in (E)–(H), (K), (I), (N), and (P)–(R) are provided in Table S1. Data are presented as mean  $\pm$  SEM. ns, not significant; \* $p < 0.05$ , \*\* $p < 0.01$ , \*\*\* $p < 0.001$ .

projections to respiratory-related nuclei such as the NTS, ventrolateral medulla, LPBN, and LC, reflecting the respiratory nature of sniffing.<sup>58,59</sup>

Based on featured projections of OVLT<sup>Glut</sup> neurons, we determined their potential downstream targets involved in the central respiratory drive that underlies sniffing episodes. In anesthetized mice, photostimulation of axonal terminals of the OVLT<sup>Glut</sup> neurons in the PVN, LH, DMH, and SFO, but not in the LPBN, LC, pre-BötC, and NTS, significantly increased in the frequency of PND without altering their amplitude. Moreover, in conscious mice, photostimulation of OVLT<sup>Glut</sup> axonal terminals in the PVN, compared to those in the LH, DMH, and SFO, elicited intense sniffing, accompanied by increased BF, PIF, and sniffing duration. In contrast, selective lesions of PVN neurons projecting to the preBötC significantly inhibited the occurrence of sniffing induced both by photostimulation of OVLT<sup>Glut</sup> neurons projecting to the PVN and by i.p. injection of hypertonic saline. Furthermore, we provide neural tracing and electrophysiological evidence that OVLT<sup>Glut</sup> neurons projecting to the PVN have established monosynaptic connections with PVN neurons projecting to the pre-BötC. Photostimulation of OVLT<sup>Glut</sup> neurons induced sniffing through either monosynaptic or polysynaptic transmission between the OVLT<sup>Glut</sup> neurons projecting to the PVN and PVN neurons projecting to the preBötC, or both. Collectively, these findings strongly suggest that OVLT<sup>Glut</sup> neuron activation produces sniffing via an OVLT<sup>Glut</sup>-PVN-preBötC circuit, highlighting the importance of this pathway in the regulation of thirst-driven respiratory behaviors.

### Exploratory sniffing facilitates the efficiency of water seeking

Rodents have evolved a variety of strategies to seek water sources, encompassing physiological demands (thirst motivation), sensory (taste) mechanisms, and behavioral (sniffing) activities. In mammals, specific neural populations within the circumventricular organs of the brain detect internal water balance and regulate water intake. Recent studies have shown that water detection is, in part, encoded by the taste system.<sup>60</sup> Sniffing and whisking help rodents to rapidly and precisely locate and track objects in their environment.<sup>4</sup> Therefore, sniffing is considered a pivotal exploratory behavior for water seeking. However, the circuit mechanisms by which different internal states drive exploratory sniffing behaviors are lacking in data.

In the present study, we provide two key findings regarding the neural mechanisms underlying thirst-driven exploratory sniffing in rodents. First, both hypertonic stimulation and activation of OVLT<sup>Glut</sup> neurons can induce robust sniffing behavior. While it is well established that several brain regions, including brainstem respiratory centers, are involved in the generation of sniffing, our findings pinpoint a critical interoceptive target for initiating thirst-motivated sniffing. This suggests that OVLT<sup>Glut</sup> neurons play a pivotal role in translating internal signals of dehydration into exploratory behaviors. Second, our findings suggest a three-order circuit for thirst-driven sniffing: the OVLT-PVN-preBötC pathway. This circuit encompasses interoceptive neurons, integration/relay neurons, and respiratory neurons, highlighting a sequential and specialized neural processing mechanism. Specifically, OVLT<sup>Glut</sup> neurons function

as thirst-sensing cells, which detect and respond to hypertonic stimuli in the body. The PVN neurons then integrate and relay these inputs, facilitating the transmission of thirst-related signals to the preBötC. Finally, the preBötC, a key respiratory control center, generates a specialized breathing pattern—sniffing—that is critical for efficient water-seeking behaviors. The OVLT-PVN-preBötC circuit is instrumental in the regulation of water-seeking efficiency through exploratory sniffing. This circuit enables rodents to rapidly respond to individual demand for hydration and to environmental changes, thereby enhancing their survival and adaptive capabilities.

### Limitations of the study

Our study demonstrates that activating the OVLT<sup>Glut</sup>-PVN-preBötC circuit induces thirst-driven exploratory sniffing, while the potential effects of GABAergic neurons in the OVLT necessitate further investigation. Moreover, previous research shows that the MnPO plays a central role in producing thirst-motivational drive.<sup>38</sup> However, distinguishing between OVLT and MnPO neurons in our study remains a challenge due to their proximal location. Given the anatomical proximity, it is impossible to rule out the possibility that MnPO neurons also contribute to the regulation of thirst-driven sniffing. In addition, while our data indicate a direct pathway from the PVN to the preBötC in the regulation of sniffing behavior, we cannot exclude the possibility that the PVN may also regulate sniffing through indirect pathways. Nonetheless, our findings show that the sniffing behavior induced by stimulating the axon terminals of OVLT<sup>Glut</sup> neurons within the PVN can be effectively abolished by lesioning the PVN neurons that project to the preBötC. This provides strong evidence for the importance of the direct connection between the PVN and preBötC in mediating thirst-driven exploratory sniffing.

### Conclusion

In summary, our study presents the OVLT<sup>Glut</sup>-PVN-preBötC pathway as the neural circuitry basis for the generation of thirst-driven sniffing in mice when exposed to hypertonic stimulation. This sniffing behavior is a vital survival mechanism that enhances environmental sampling and improves water-seeking efficiency. The OVLT-PVN-preBötC circuit represents a well-defined pathway that integrates internal thirst signals with respiratory motor outputs, underscoring the intricate interplay between sensory input and behavioral responses in rodents.

### RESOURCE AVAILABILITY

#### Lead contact

Further information and requests for resources should be directed to and will be fulfilled by the lead contact, Sheng Wang ([wangsheng@hebmu.edu.cn](mailto:wangsheng@hebmu.edu.cn)).

#### Materials availability

- No unique mouse lines have been generated in this study.
- This study did not generate new unique reagents.

#### Data and code availability

- All data reported in this study will be shared by the [lead contact](#) upon request.
- All original code has been deposited at Zenodo and is publicly available at <https://doi.org/10.5281/zenodo.14545435> as of the date of publication.

- Any additional information required to reanalyze the data reported in this study is available from the [lead contact](#) upon request.

## ACKNOWLEDGMENTS

This work was supported by grants from the National Natural Science Foundation of China (grants U23A20431, 32171126, 82100458) and the Natural Science Foundation of Hebei Province for Innovative Research Grant Group Project (H2021206203). The authors are grateful to the Core Facilities and Centers in Hebei Medical University. [Figures 1, 3, 6, and S1](#) as well as the graphical abstract were created using [BioRender.com](#).

## AUTHOR CONTRIBUTIONS

W.H., L.S., and S.W. designed the research. W.H., Z.Y., K.Z., K.W., and T.D. performed all the physiological experiments. X.T., X.Z., X.M., and Y.C. conducted all histological preparations. X.W., X.J., and S.B. analyzed data. L.S., F.Y., and S.W. wrote the paper. All authors approved the final version of the manuscript.

## DECLARATION OF INTERESTS

The authors declare no competing interests.

## STAR★METHODS

Detailed methods are provided in the online version of this paper and include the following:

- KEY RESOURCES TABLE
- EXPERIMENTAL MODEL AND STUDY PARTICIPANT DETAILS
  - Animals
- METHOD DETAILS
  - Recordings of sniffing
  - Stereotaxic viral injections
  - Fiber photometry
  - Optogenetics
  - PND recording
  - Drinking latency
  - Patch-clamp recording
  - Immunohistochemistry and RNAscope
- QUANTIFICATION AND STATISTICAL ANALYSIS

## SUPPLEMENTAL INFORMATION

Supplemental information can be found online at <https://doi.org/10.1016/j.celrep.2025.115254>.

Received: July 13, 2024

Revised: January 9, 2025

Accepted: January 10, 2025

Published: February 1, 2025

## REFERENCES

- Wachowiak, M. (2010). Active Sensing in Olfaction. In *The Neurobiology of Olfaction*, A. Menini, ed.
- Schaefer, A.T., and Margrie, T.W. (2007). Spatiotemporal representations in the olfactory system. *Trends Neurosci.* 30, 92–100. <https://doi.org/10.1016/j.tins.2007.10.001>.
- Wachowiak, M. (2011). All in a sniff: olfaction as a model for active sensing. *Neuron* 71, 962–973. <https://doi.org/10.1016/j.neuron.2011.08.030>.
- Deschenes, M., Moore, J., and Kleinfeld, D. (2012). Sniffing and whisking in rodents. *Curr. Opin. Neurobiol.* 22, 243–250. <https://doi.org/10.1016/j.conb.2011.11.013>.
- Moore, J.D., Deschenes, M., Furuta, T., Huber, D., Smear, M.C., Demers, M., and Kleinfeld, D. (2013). Hierarchy of orofacial rhythms revealed through whisking and breathing. *Nature* 497, 205–210. <https://doi.org/10.1038/nature12076>.
- Photopoulos, J. (2022). The dogs learning to sniff out disease. *Nature* 606, S10–S11. <https://doi.org/10.1038/d41586-022-01629-8>.
- Wesson, D.W. (2013). Sniffing behavior communicates social hierarchy. *Curr. Biol.* 23, 575–580. <https://doi.org/10.1016/j.cub.2013.02.012>.
- Kepcs, A., Uchida, N., and Mainen, Z.F. (2006). The sniff as a unit of olfactory processing. *Chem. Senses* 31, 167–179. <https://doi.org/10.1093/chemse/bjj016>.
- Ravreby, I., Snitz, K., and Sobel, N. (2022). There is chemistry in social chemistry. *Sci. Adv.* 8, eabn0154. <https://doi.org/10.1126/sciadv.abn0154>.
- Catania, K.C. (2006). Olfaction: underwater ‘sniffing’ by semi-aquatic mammals. *Nature* 444, 1024–1025. <https://doi.org/10.1038/4441024a>.
- Bhandare, A., van de Wiel, J., Roberts, R., Braren, I., Huckstepp, R., and Dale, N. (2022). Analyzing the brainstem circuits for respiratory chemosensitivity in freely moving mice. *Elife* 11, e70671. <https://doi.org/10.7554/elife.70671>.
- Deschenes, M., Kurnikova, A., Elbaz, M., and Kleinfeld, D. (2016). Circuits in the Ventral Medulla That Phase-Lock Motoneurons for Coordinated Sniffing and Whisking. *Neural Plast.* 2016, 7493048. <https://doi.org/10.1155/2016/7493048>.
- Silva, J.N., Oliveira, L.M., Souza, F.C., Moreira, T.S., and Takakura, A.C. (2019). Distinct pathways to the parafacial respiratory group to trigger active expiration in adult rats. *Am. J. Physiol. Lung Cell Mol. Physiol.* 317, L402–L413. <https://doi.org/10.1152/ajplung.00467.2018>.
- Alexandrov, V.G., Ivanova, T.G., and Alexandrova, N.P. (2007). Prefrontal control of respiration. *J. Physiol. Pharmacol.* 58, 17–23.
- Sobel, N., Prabhakaran, V., Desmond, J.E., Glover, G.H., Goode, R.L., Sullivan, E.V., and Gabrieli, J.D. (1998). Sniffing and smelling: separate subsystems in the human olfactory cortex. *Nature* 392, 282–286. <https://doi.org/10.1038/32654>.
- Savic, I. (2002). Imaging of brain activation by odorants in humans. *Curr. Opin. Neurobiol.* 12, 455–461. [https://doi.org/10.1016/s0959-4388\(02\)00346-x](https://doi.org/10.1016/s0959-4388(02)00346-x).
- Ikemoto, S., and Panksepp, J. (1994). The relationship between self-stimulation and sniffing in rats: does a common brain system mediate these behaviors? *Behav. Brain Res.* 61, 143–162. [https://doi.org/10.1016/0166-4328\(94\)90155-4](https://doi.org/10.1016/0166-4328(94)90155-4).
- Allen, W.E., Chen, M.Z., Pichamoothy, N., Tien, R.H., Pachitariu, M., Luo, L., and Deisseroth, K. (2019). Thirst regulates motivated behavior through modulation of brainwide neural population dynamics. *Science* 364, 253. <https://doi.org/10.1126/science.aav3932>.
- McKinley, M.J., McAllen, R.M., Davern, P., Giles, M.E., Penschow, J., Sunn, N., Uschakov, A., and Oldfield, B.J. (2003). The sensory circumventricular organs of the mammalian brain. *Adv. Anat. Embryol. Cell Biol.* 172, 1–122, back cover. <https://doi.org/10.1007/978-3-642-55532-9>.
- Pool, A.H., Wang, T., Stafford, D.A., Chance, R.K., Lee, S., Ngai, J., and Oka, Y. (2020). The cellular basis of distinct thirst modalities. *Nature* 588, 112–117. <https://doi.org/10.1038/s41586-020-2821-8>.
- Buggy, J., and Jonhson, A.K. (1977). Preoptic-hypothalamic periventricular lesions: thirst deficits and hypernatremia. *Am. J. Physiol.* 233, R44–R52. <https://doi.org/10.1152/ajpregu.1977.233.1.R44>.
- McKinley, M.J., Yao, S.T., Uschakov, A., McAllen, R.M., Rundgren, M., and Martelli, D. (2015). The median preoptic nucleus: front and centre for the regulation of body fluid, sodium, temperature, sleep and cardiovascular homeostasis. *Acta Physiol.* 214, 8–32. <https://doi.org/10.1111/apha.12487>.
- Gizowski, C., and Bourque, C.W. (2018). The neural basis of homeostatic and anticipatory thirst. *Nat. Rev. Nephrol.* 14, 11–25. <https://doi.org/10.1038/nrneph.2017.149>.

24. Kinsman, B.J., Simmonds, S.S., Browning, K.N., and Stocker, S.D. (2017). Organum Vasculosum of the Lamina Terminalis Detects NaCl to Elevate Sympathetic Nerve Activity and Blood Pressure. *Hypertension* 69, 163–170. <https://doi.org/10.1161/HYPERTENSIONAHA.116.08372>.
25. Nomura, K., Hiyama, T.Y., Sakuta, H., Matsuda, T., Lin, C.H., Kobayashi, K., Kobayashi, K., Kuwaki, T., Takahashi, K., Matsui, S., and Noda, M. (2019). [Na(+)] Increases in Body Fluids Sensed by Central Nax Induce Sympathetically Mediated Blood Pressure Elevations via H(+) -Dependent Activation of ASIC1a. *Neuron* 101, 60–75.e6. <https://doi.org/10.1016/j.neuron.2018.11.017>.
26. Sakuta, H., Lin, C.H., Yamada, M., Kita, Y., Tokuoka, S.M., Shimizu, T., and Noda, M. (2020). Na(x)-positive glial cells in the organum vasculosum laminæ terminalis produce epoxyeicosatrienoic acids to induce water intake in response to increases in [Na<sup>+</sup>] in body fluids. *Neurosci. Res.* 154, 45–51. <https://doi.org/10.1016/j.neures.2019.05.006>.
27. Sakuta, H., Lin, C.H., Hiyama, T.Y., Matsuda, T., Yamaguchi, K., Shigenobu, S., Kobayashi, K., and Noda, M. (2020). SLC9A4 in the organum vasculosum of the lamina terminalis is a [Na<sup>+</sup>] sensor for the control of water intake. *Pflügers Archiv* 472, 609–624. <https://doi.org/10.1007/s00424-020-02389-y>.
28. Matsuda, T., Hiyama, T.Y., Niimura, F., Matsusaka, T., Fukamizu, A., Kobayashi, K., Kobayashi, K., and Noda, M. (2017). Distinct neural mechanisms for the control of thirst and salt appetite in the subfornical organ. *Nat. Neurosci.* 20, 230–241. <https://doi.org/10.1038/nn.4463>.
29. Zimmerman, C.A., Leib, D.E., and Knight, Z.A. (2017). Neural circuits underlying thirst and fluid homeostasis. *Nat. Rev. Neurosci.* 18, 459–469. <https://doi.org/10.1038/nrn.2017.71>.
30. Kurnikova, A., Moore, J.D., Liao, S.M., Deschênes, M., and Kleinfeld, D. (2017). Coordination of Orofacial Motor Actions into Exploratory Behavior by Rat. *Curr. Biol.* 27, 688–696. <https://doi.org/10.1016/j.cub.2017.01.013>.
31. Yang, C.F., Kim, E.J., Callaway, E.M., and Feldman, J.L. (2020). Mono-synaptic Projections to Excitatory and Inhibitory preBötzingers Complex Neurons. *Front. Neuroanat.* 14, 58. <https://doi.org/10.3389/fnana.2020.00058>.
32. Tsai, N.Y., Wang, F., Toma, K., Yin, C., Takatoh, J., Pai, E.L., Wu, K., Matcham, A.C., Yin, L., Dang, E.J., et al. (2022). Trans-Seq maps a selective mammalian retinotectal synapse instructed by Nephronectin. *Nat. Neurosci.* 25, 659–674. <https://doi.org/10.1038/s41593-022-01068-8>.
33. Mack, S.O., Wu, M., Kc, P., and Haxhiu, M.A. (2007). Stimulation of the hypothalamic paraventricular nucleus modulates cardiorespiratory responses via oxytocinergic innervation of neurons in pre-Bötzingers complex. *J. Appl. Physiol.* 102, 189–199. <https://doi.org/10.1152/japplphysiol.00522.2006>.
34. Uchida, N., Kepcs, A., and Mainen, Z.F. (2006). Seeing at a glance, smelling in a whiff: rapid forms of perceptual decision making. *Nat. Rev. Neurosci.* 7, 485–491. <https://doi.org/10.1038/nrn1933>.
35. Brudner, S., and Emonet, T. (2022). Where is that smell coming from? *Elife* 11, e82635. <https://doi.org/10.7554/elife.82635>.
36. Lin, S., Owald, D., Chandra, V., Talbot, C., Huettneroth, W., and Waddell, S. (2014). Neural correlates of water reward in thirsty Drosophila. *Nat. Neurosci.* 17, 1536–1542. <https://doi.org/10.1038/nn.3827>.
37. Giziowski, C., and Bourque, C.W. (2020). Sodium regulates clock time and output via an excitatory GABAergic pathway. *Nature* 583, 421–424. <https://doi.org/10.1038/s41586-020-2471-x>.
38. Allen, W.E., DeNardo, L.A., Chen, M.Z., Liu, C.D., Loh, K.M., Fenno, L.E., Ramakrishnan, C., Deisseroth, K., and Luo, L. (2017). Thirst-associated preoptic neurons encode an aversive motivational drive. *Science* 357, 1149–1155. <https://doi.org/10.1126/science.aan6747>.
39. Kucharczyk, J., Assaf, S.Y., and Mogenson, G.J. (1976). Differential effects of brain lesions on thirst induced by the administration of angiotensin-II to the preoptic region, subfornical organ and anterior third ventricle. *Brain Res.* 108, 327–337. [https://doi.org/10.1016/0006-8993\(76\)90189-x](https://doi.org/10.1016/0006-8993(76)90189-x).
40. Thrasher, T.N., Simpson, J.B., and Ramsay, D.J. (1982). Lesions of the subfornical organ block angiotensin-induced drinking in the dog. *Neuroendocrinology* 35, 68–72. <https://doi.org/10.1159/000123357>.
41. Johnson, A.K., and Buggy, J. (1978). Periventricular preoptic-hypothalamus is vital for thirst and normal water economy. *Am. J. Physiol.* 234, R122–R129. <https://doi.org/10.1152/ajpregu.1978.234.3.R122>.
42. Thrasher, T.N., Keil, L.C., and Ramsay, D.J. (1982). Lesions of the organum vasculosum of the lamina terminalis (OVLT) attenuate osmotically-induced drinking and vasopressin secretion in the dog. *Endocrinology* 110, 1837–1839. <https://doi.org/10.1210/endo-110-5-1837>.
43. Farrell, M.J., Bowala, T.K., Gavrilescu, M., Phillips, P.A., McKinley, M.J., McAllen, R.M., Denton, D.A., and Egan, G.F. (2011). Cortical activation and lamina terminalis functional connectivity during thirst and drinking in humans. *Am. J. Physiol. Regul. Integr. Comp. Physiol.* 301, R623–R631. <https://doi.org/10.1152/ajpregu.00817.2010>.
44. Egan, G., Silk, T., Zamarripa, F., Williams, J., Federico, P., Cunningham, R., Carabott, L., Blair-West, J., Shade, R., McKinley, M., et al. (2003). Neural correlates of the emergence of consciousness of thirst. *Proc. Natl. Acad. Sci. USA* 100, 15241–15246. <https://doi.org/10.1073/pnas.2136650100>.
45. Abbott, S.B.G., Machado, N.L.S., Geerling, J.C., and Saper, C.B. (2016). Reciprocal Control of Drinking Behavior by Median Preoptic Neurons in Mice. *J. Neurosci.* 36, 8228–8237. <https://doi.org/10.1523/jneurosci.1244-16.2016>.
46. Augustine, V., Gokce, S.K., Lee, S., Wang, B., Davidson, T.J., Reimann, F., Gribble, F., Deisseroth, K., Lois, C., and Oka, Y. (2018). Hierarchical neural architecture underlying thirst regulation. *Nature* 555, 204–209. <https://doi.org/10.1038/nature25488>.
47. Perez de Los Cobos Pallares, F., Bautista, T.G., Stanic, D., Egger, V., and Dutschmann, M. (2016). Brainstem-mediated sniffing and respiratory modulation during odor stimulation. *Respir. Physiol. Neurobiol.* 233, 17–24. <https://doi.org/10.1016/j.resp.2016.07.008>.
48. Hu, H., Cui, Y., and Yang, Y. (2020). Circuits and functions of the lateral habenula in health and in disease. *Nat. Rev. Neurosci.* 21, 277–295. <https://doi.org/10.1038/s41583-020-0292-4>.
49. Sternson, S.M. (2013). Hypothalamic survival circuits: blueprints for purposive behaviors. *Neuron* 77, 810–824. <https://doi.org/10.1016/j.neuron.2013.02.018>.
50. Schwartz, M.W., Woods, S.C., Porte, D., Jr., Seeley, R.J., and Baskin, D.G. (2000). Central nervous system control of food intake. *Nature* 404, 661–671. <https://doi.org/10.1038/35007534>.
51. Nakamura, K., Nakamura, Y., and Kataoka, N. (2022). A hypothalamomodulatory network for physiological responses to environmental stresses. *Nat. Rev. Neurosci.* 23, 35–52. <https://doi.org/10.1038/s41583-021-0532-x>.
52. Fukushi, I., Yokota, S., and Okada, Y. (2019). The role of the hypothalamus in modulation of respiration. *Respir. Physiol. Neurobiol.* 265, 172–179. <https://doi.org/10.1016/j.resp.2018.07.003>.
53. Breton-Provencher, V., and Sur, M. (2019). Active control of arousal by a locus coeruleus GABAergic circuit. *Nat. Neurosci.* 22, 218–228. <https://doi.org/10.1038/s41593-018-0305-z>.
54. Nagashima, T., Tohyama, S., Mikami, K., Nagase, M., Morishima, M., Kasai, A., Hashimoto, H., and Watabe, A.M. (2022). Parabrachial-to-parasubthalamus nucleus pathway mediates fear-induced suppression of feeding in male mice. *Nat. Commun.* 13, 7913. <https://doi.org/10.1038/s41467-022-35634-2>.
55. Morales, M., and Margolis, E.B. (2017). Ventral tegmental area: cellular heterogeneity, connectivity and behaviour. *Nat. Rev. Neurosci.* 18, 73–85. <https://doi.org/10.1038/nrn.2016.165>.
56. Liu, Z., Lin, R., and Luo, M. (2020). Reward Contributions to Serotonergic Functions. *Annu. Rev. Neurosci.* 43, 141–162. <https://doi.org/10.1146/annurev-neuro-093019-112252>.

57. Roman-Ortiz, C., Guevara, J.A., and Clem, R.L. (2021). GABAergic basal forebrain projections to the periaqueductal gray promote food consumption, reward and predation. *Sci. Rep.* 11, 22638. <https://doi.org/10.1038/s41598-021-02157-7>.
58. Yackle, K. (2023). Transformation of Our Understanding of Breathing Control by Molecular Tools. *Annu. Rev. Physiol.* 85, 93–113. <https://doi.org/10.1146/annurev-physiol-021522-094142>.
59. Yackle, K., Schwarz, L.A., Kam, K., Sorokin, J.M., Huguenard, J.R., Feldman, J.L., Luo, L., and Krasnow, M.A. (2017). Breathing control center neurons that promote arousal in mice. *Science* 355, 1411–1415. <https://doi.org/10.1126/science.aai7984>.
60. Zocchi, D., Wennemuth, G., and Oka, Y. (2017). The cellular mechanism for water detection in the mammalian taste system. *Nat. Neurosci.* 20, 927–933. <https://doi.org/10.1038/nn.4575>.
61. Yu, H., Shi, L., Chen, J., Jun, S., Hao, Y., Wang, S., Fu, C., Zhang, X., Lu, H., Wang, S., and Yuan, F. (2022). A Neural Circuit Mechanism Controlling Breathing by Leptin in the Nucleus Tractus Solitarii. *Neurosci. Bull.* 38, 149–165. <https://doi.org/10.1007/s12264-021-00742-4>.
62. Keller, J.A., Chen, J., Simpson, S., Wang, E.H.J., Lilascharoen, V., George, O., Lim, B.K., and Stowers, L. (2018). Voluntary urination control by brain-stem neurons that relax the urethral sphincter. *Nat. Neurosci.* 21, 1229–1238. <https://doi.org/10.1038/s41593-018-0204-3>.

## STAR★METHODS

### KEY RESOURCES TABLE

| REAGENT or RESOURCE  | SOURCE   | IDENTIFIER   |
|--|--|--|
| <b>Antibodies</b>  |  |  |
| Guinea Pig anti-cFos   | Synaptic Systems   | Cat # 226308; RRID: AB_2905595   |
| Chicken anti-GFP   | Abcam  | Cat # ab13970; RRID: AB_300798   |
| Rabbit anti-mCherry  | Novus Biologicals  | Cat # NBP2-25157; RRID: AB_2753204   |
| CyTM3 Goat Anti-Guinea Pig IgG (H + L)                                 | Jackson ImmunoResearch Laboratories                      | Cat # 106-165-003; RRID: AB_2337423  |
| CyTM3 AffiniPure goat anti-rabbit IgG (H + L)                          | Jackson ImmunoResearch Laboratories                      | Cat # 111-165-003; RRID: AB_2338000  |
| Alexa Fluor® 488 goat polyclonal secondary antibody to chicken IgY-H&L | Abcam  | Cat # ab150169; RRID: AB_2636803   |
| <b>Bacterial and virus strains</b>                                     |  |  |
| rAAV9-Syn-DIO-GCaMP6S  | Brain Case   | Cat # BC-0086<br>2.5E + 12VG/ml  |
| AAV9-EF1 $\alpha$ -DIO-ChR2-mCherry                                    | Genechem   | Cat # GCPV0391264<br>6.27E + 13VG/ml   |
| rAAV9-EF1 $\alpha$ -DIO-eNpHR3.0-EYFP                                  | BrainVTA   | Cat # PT-006<br>5.73E + 12VG/ml  |
| AAV8-hSyn-DIO-mCherry  | Genechem   | Cat # 25917<br>1.04E + 13VG/ml   |
| AAV9-EF1 $\alpha$ -DIO-EYFP  | Genechem   | Cat # 19870<br>1.04E + 13VG/ml   |
| AAV9-CAG-DIO-mWGA-Flpo   | Brain Case   | Cat # BC-1400<br>5.01E + 12VG/ml   |
| AAV8-hSyn-fDIO-EYFP  | Brain Case   | Cat # BC-0477<br>2.50E + 12VG/ml   |
| AAV9-EF1 $\alpha$ -fDIO-taCasp3-TEVP-WPRE-PA                           | Taitool Bioscience                                       | Cat # S0302-9<br>1.00E + 13VG/ml   |
| AAVretro-hSyn-mCherry  | Genechem   | Cat # NOGCPV0405840<br>3.49E + 13VG/ml   |
| AAVretro-hSyn-EYFP   | Genechem   | Cat # 25876-11<br>1.5E + 13VG/ml   |
| AAVretro-hSyn-Flpo-EYFP  | Genechem   | Cat # GOSV0331986<br>1.00E + 12VG/ml   |
| AAVretro-EF1 $\alpha$ -hChR2-EYFP                                      | Brain Case   | Cat # BC-0107<br>5.20E + 12VG/ml   |
| <b>Experimental models: Organisms/strains</b>                          |  |  |
| C57BL/6J   | Beijing Vital River Laboratory Animal Technology Company | 219  |
| Vglut2-Cre   | The Jackson Laboratory                                   | RRID: IMSR_JAX:016963  |
| <b>Software and algorithms</b>   |  |  |
| Finepointe software  | DSI  | <a href="http://www.datasci.com/products/buxco-respiratory-products/finepointe-whole-body-plethysmography">www.datasci.com/products/<br/>buxco-respiratory-products/finepointe-<br/>whole-body-plethysmography</a> |
| Spike 2  | Cambridge Electronic Design                              | <a href="http://ced.co.uk">ced.co.uk</a>   |
| MATLAB   | MathWorks  | <a href="http://www.mathworks.com">www.mathworks.com</a>   |
| custom-made MATLAB scripts   | ThinkerTech  | <a href="http://zenodo.org/records/14545435">zenodo.org/records/14545435</a>   |
| pClamp 10  | Molecular Devices  | <a href="http://www.moleculardevices.com">www.moleculardevices.com</a>   |
| ZEN  | Zeiss  | <a href="http://www.zeiss.com.cn/micro">www.zeiss.com.cn/micro</a>   |
| Prism 9  | GraphPad   | <a href="http://www.graphpad-prism.cn">www.graphpad-prism.cn</a>   |

(Continued on next page)

**Continued**

| REAGENT or RESOURCE     | SOURCE                        | IDENTIFIER                     |
|-------------------------|-------------------------------|--------------------------------|
| ImageJ                  | National Institutes of Health | ImageJ.net<br>RRID: SCR_003070 |
| <b>Other</b>            |                               |                                |
| probe <i>Slc17a6</i>    | Advanced Cell Diagnostics     | Cat # 319171                   |
| probe <i>Slc32a1-C3</i> | Advanced Cell Diagnostics     | Cat # 319191-C3                |

**EXPERIMENTAL MODEL AND STUDY PARTICIPANT DETAILS****Animals**

Mice were acquired from Beijing Vital River Laboratory Animal Technology Company (C57BL/6J wild-type) and the Jackson Laboratory (Vglut2-Cre, RRID: IMSR\_JAX:016963). The mice were then housed and bred in an SPF facility at  $22 \pm 2^\circ\text{C}$  and  $50\% \pm 2\%$  humidity with 12 h light/dark cycle, with *ad libitum* access to food and water. Unless otherwise stated, all studies employed a mixture of male and female (8–12 weeks of age) mice and no differences between sexes were observed. Animal handling and experimental procedures were in accordance with the Guide for the Care and Use of Laboratory Animals, and approved by the Animal Care and Ethics Committee of Hebei Medical University (Hebmu-P2023052).

**METHOD DETAILS****Recordings of sniffing**

We recorded sniffing using a whole-body plethysmography (Buxco, Wilmington, NC) in freely moving mice as described previously.<sup>3,59,61</sup> A mass flow regulator provides quiet, constant and smooth room air through a chamber (0.5 L/min). Airflow signals were recorded, amplified, digitized and analyzed by Finepointe software (Buxco Research Systems, Wilmington, NC). Eupneic breathing measured during behavioral quiescence is defined as 3 or more breaths in a row at a BF less than 5 Hz. Sniffing is defined as 4 or more breaths in a row at  $\text{BF} \geq 7 \text{ Hz}$  and  $\text{PIF} \geq 7 \text{ mL/s}$ .<sup>59</sup> Mice were habituated to plethysmograph chambers with food and water available for at least 2 h per day for 5 days consecutively before the experiment and showed at least 10 min of eupneic breathing before testing. To elicit thirst-driven sniff behavior rapidly, 2 M NaCl (8  $\mu\text{L/g}$  body weight)<sup>37</sup> was injected intraperitoneally (i.p.), and an equal amount of saline as a control. Other parameters, such as the onset of water drinking and the timing of water seeking and drinking, were monitored by video recording.

**Stereotaxic viral injections**

Viral injection surgeries were performed under pentobarbital sodium (60 mg/kg body weight, i.p.) anesthesia, with the animal positioned in a stereotaxic frame (RWD Life Science, China), similar to previously described methods.<sup>61</sup> Anesthetic depth was assessed via toe pinch, and supplemental anesthesia (30% of the initial dose, i.p.) was administered as needed. The body temperature was maintained at  $37^\circ\text{C}$  using a program-controlled heating pad, while the eyes were protected with ophthalmic ointment to prevent dryness. Under aseptic conditions, the skull was exposed via a small incision, and a hole ( $\sim 0.5 \text{ mm}$  drill bit) was drilled above the injection sites. All injections were performed with a pulled-glass pipette (25  $\mu\text{m}$  in diameter) connected to a Hamilton syringe (2  $\mu\text{L}$ ), which was driven by a microinjector pump (Harvard Apparatus, USA), at a rate of 0.1  $\mu\text{L}/\text{min}$ . After the injection, the pipette was left in place for at least 5 min before withdrawal and the scalp was closed with sutures. After surgery, each mouse was administered an analgesic, ketorolac (4 mg/kg, i.p.), and an antibiotic, ampicillin (125 mg/kg, i.p.), immediately. Animals were allowed to recover for at least 3 weeks after surgery before continuing experiments.

In order to visualize and control the activity of OVLT<sup>Glut</sup> neurons *in vivo*, we targeted the OVLT region (bregma: 0.86 mm anterior, 0 mm lateral, and  $-5.26 \text{ mm}$  ventral) in Vglut2-cre mice. We then injected 100 nL of rAAV9-Syn-DIO-GCaMP6s for calcium imaging, 60 nL of AAV9-EF1 $\alpha$ -DIO-ChR2-mCherry or AAV9-EF1 $\alpha$ -DIO-eNpHR3.0-EYFP for optical manipulation, and AAV8-hSyn-DIO-mCherry or AAV9-EF1 $\alpha$ -DIO-EYFP for control experiments.

To identify PVN neurons that received inputs from the OVLT<sup>Glut</sup> neurons, we employed anterograde trans-synaptic tracing by injecting AAV9-CAG-DIO-mWGA-Flpo (60 nL) into the OVLT region and AAV8-hSyn-fDIO-EYFP (100 nL) into the unilateral PVN region (bregma:  $-0.44 \text{ mm}$  posterior, 0.15 mm lateral, and  $-4.90 \text{ mm}$  ventral) of Vglut2-cre mice. Additionally, the retrograde tracing virus AAVretro-EF1 $\alpha$ -mCherry (100 nL) was injected into the preBötC on the same side as the PVN (bregma:  $-6.95 \text{ mm}$  posterior, 1.38 mm lateral, and  $-5.90 \text{ mm}$  ventral), allowing for precise labeling of PVN neurons projecting to the preBötC.

To verify the PVN-preBötC circuit is involved in the regulation of respiration, AAVretro-EF1 $\alpha$ -mCherry (100 nL) was bilaterally injected into the preBötC. For patch-clamp recording, 60 nL of AAV9-EF1 $\alpha$ -DIO-ChR2-mCherry was injected into the OVLT, and 100 nL of AAVretro-hSyn-EYFP was bilaterally injected into the preBötC.

The specific disruption of synaptic connections between PVN and preBötC was achieved by bilaterally injecting 100 nL of AAV9-EF1a-fDIO-taCasp3 in the PVN region and 100 nL of AAVretro-hSyn-Flpo-EYFP in the preBötC, enabling the specific interference of synaptic connections between PVN and preBötC on both sides. Additional information on viral vectors is available in the key resources table.

### Fiber photometry

Real-time fluorescence emitted from the calcium sensor GCaMP6s, expressed by OVLT<sup>Glut</sup> neurons, was recorded using fiber photometry (ThinkerTech, Nanjing, China), as previously described in the literature.<sup>62</sup> After viral infections, a custom-made optic fiber (200 μm core diameter, 0.37 NA) was implanted 100 μm above the OVLT immediately and secured in place with metabond and dental cement. For fiber photometry recordings, a 1.5-meter-long fiber-optic patch cord was connected to the chronically implanted optical fiber and suspended above the plethysmograph chambers to allow animals to freely interact and move during the experiment. Experiments were done at least 3 weeks after viral injection to allow for sufficient viral. Photometry data were analyzed offline using Spike2 software and custom-made MATLAB scripts. The instantaneous change in fluorescence ( $\Delta F/F_0$ ) was calculated as  $(V_{\text{signal}} - F_0)/(F_0 - V_{\text{offset}})$ .  $V_{\text{signal}}$  is defined as the measured fluorescence signal intensity. This is the fluorescence intensity value at the current time point.  $F_0$ : the baseline fluorescence signal intensity, usually measured under relatively quiet mice.  $V_{\text{offset}}$ : an offset value used to correct for background fluorescence or other non-calcium-related fluorescence signals. Given the compact size of the OVLT, the viral injection center and optic fiber track of each mouse was confirmed in the present study. The mice without correct targeting of the OVLT were rejected without further analysis. Custom MATLAB (MathWorks, Natick, USA) scripts produced by ThinkerTech.

### Optogenetics

For optogenetic manipulation of OVLT<sup>Glut</sup> neurons in freely moving mice, a ceramic ferrule with an optic fiber (200 μm in diameter, N.A. 0.22) was implanted and anchored to skull using dental cement, with the fiber tip positioned 100 μm above the OVLT immediately after the injections of viruses. The optogenetic experiments were conducted at least 3 weeks after optic fiber implantation. For photostimulation, blue (473 nm) or yellow (589 nm) laser light was delivered via a fiber optic patch cord (Doric Lenses), which was connected to a dual channel Optogenetic Smart Light Source (Aurora-400, Newdoon Inc., China). Blue light (473 nm, 10 Hz, 20 ms pulse width, 1 s duration, 3 s intervals) was delivered for 10 min to activate OVLT<sup>Glut</sup> neurons and trigger sniffing. Continuous yellow light (589 nm, 10 mW) was delivered immediately after injection of 2 M NaCl (i.p.) for 30 min to achieve long-term inhibition of OVLT<sup>Glut</sup> neurons.

During PND experiments that employed optogenetic activation of OVLT<sup>Glut</sup> neurons and their axons, optical fibers were not pre-implanted in the mice used for optogenetic experiments under anesthesia. Three weeks after virus injection, the mice were fixed in a stereotaxic frame, and PND recordings with optogenetic stimulation were performed under urethane (1.3 g/kg body weight, i.p.) anesthesia. A fiber optic cable and cannulae (200 μm diameter) were attached to the stereotaxic arm to target and stimulate specific brain regions. The laser was continuously activated for 1 min with 20 ms pulses at a frequency of 10 Hz. For optogenetic activation of PVN neurons innervating preBötC, the laser was continuously switched on for 1 min with 20 ms pulses at a frequency of 1, 5, and 10 Hz.

The injection sites for the optical fibers are as follows: OVLT (bregma +0.86 mm, lateral 0 mm, ventral -5.16 mm), SFO (bregma -0.40 mm, lateral 0 mm, ventral -3.00 mm), PVN (bregma -0.44 mm, lateral ±0.15 mm, ventral -4.80 mm), LPBN (bregma -6.95 mm, lateral ±1.38 mm, ventral -5.7 mm), LH (bregma -1.00 mm, lateral ±1.00 mm, ventral -5.00 mm), DMH (bregma -1.50 mm, lateral ±0.35 mm, ventral -5.00 mm), LC (bregma -5.30 mm, lateral ±0.80 mm, ventral -4.70 mm), NTS (bregma -6.8 mm, lateral ±0.42 mm, ventral -4.70 mm), preBötC (bregma -6.95 mm, lateral ±1.38 mm, ventral -5.8 mm).

### PND recording

PND recording methods were based on our previous study.<sup>61</sup> Briefly, mice were anesthetized with urethane (1.3 g/kg body weight, i.p.), intubated with an endotracheal tube, vagotomized bilaterally, secured to a stereotaxic apparatus, paralyzed (pancuronium bromide; 2.5 mg/kg, i.p.) and artificially ventilated with 100% O<sub>2</sub> throughout surgery to inactivate peripheral chemoreceptors. End-tidal CO<sub>2</sub> (ETCO<sub>2</sub>) level, an indicator of the PaCO<sub>2</sub> in arterial blood, was continuously monitored using a capnograph (MicroCapStar, CWE Inc., USA). The basal ETCO<sub>2</sub> level was maintained at around 4% and could be adjusted through ventilation parameters as necessary. After the initial surgical procedure, the left phrenic nerve was separated from the surrounding tissues and carefully placed onto a silver bipolar electrode, then submerged in warm liquid paraffin. The recording electrode was connected to a neurolog extracellular recording amplifier (Digitimer, NL900D). The original signal was sampled at a rate of 2 kHz and filtered with a 30–3000 Hz bandpass. All analog data were processed using a micro1401 digitizer (Cambridge Electronic Design Ltd, UK) and subsequently analyzed offline using the Spike 2 software (RRID:SCR\_000903, Cambridge Electronic Design). The integrated PND was obtained by rectifying and smoothing (with a time constant of 0.1 s) the original signal. The frequency and peak amplitude of the integrated PND were measured for quantitative analysis.

### Drinking latency

Following the protocol described for the ablation of PVN neurons innervating preBötC, after viral expression, mice were acclimated for 1 h by placing them in a 15 cm diameter and 20 cm high chamber without water. Before placing the water bottle in the chamber, its

weight was recorded to measure baseline water volume. Afterward, the water bottle was displayed, and a 1-min countdown began. After 1 min, the laser was turned on for 10 min. Drinking latency was defined as the time from the onset of laser activation to the first time of water intake. After the experiment, the water bottle was weighed again to record water consumption. Events where no water was consumed within the 10-min window were not included in the statistical analysis.

### Patch-clamp recording

Acute brain slices containing the OVLT or PVN region were prepared from mice anesthetized with pentobarbital sodium (60 mg/kg body weight, i.p.) before decapitation. To ensure optimal health of slices, brains were rapidly removed and placed in ice-cold oxygenated (bubbled with 95% O<sub>2</sub> and 5% CO<sub>2</sub>) cutting solution (in mM: 260 sucrose, 3 KCl, 5 MgCl<sub>2</sub>, 1 CaCl<sub>2</sub>, 1.25 NaH<sub>2</sub>PO<sub>4</sub>, 26 NaHCO<sub>3</sub>, 10 glucose, 1 kynurenic acid) and sliced coronally at a thickness of 240 µm using a vibratome (Leica, VT1200S, Germany). Then, slices were incubated at 35°C in oxygenated aCSF (in mM: 125 NaCl, 3 KCl, 1.2 KH<sub>2</sub>PO<sub>4</sub>, 1.2 MgSO<sub>4</sub>, 25 NaHCO<sub>3</sub>, 10 D-glucose, and 2 CaCl<sub>2</sub>, pH 7.4, 300 mOsm) for a minimum of 30 min to facilitate recovery, and held at room temperature thereafter. Following at least 1 h of incubation with oxygenated aCSF, the slices were transferred to a recording chamber and continuously perfused with oxygenated aCSF at a flow rate of 1 mL/min.

To validate the activation of OVLT neurons by high osmolarity, an infusion solution of hypertonic aCSF was prepared by adding appropriate amounts of NaCl to the regular aCSF solution. The slices in the recording chamber were visualized through a fixed stage upright microscope (Olympus Inc., Japan) equipped with a 40× water-immersion objective lens and differential interference contrast optics.

Patch pipettes (4–6 MΩ) were pulled from borosilicate glass capillaries (length 75 mm, outer diameter 1.5 mm, inner diameter 1.1 mm, Sutter Instrument) using a Sutter P-97 horizontal puller. Pipettes were filled a solution containing (in mM): 10 NaCl, 130 K<sup>+</sup> gluconate, 11 EGTA, 1 CaCl<sub>2</sub>, 10 HEPES, 1 MgCl<sub>2</sub>, 2 MgATP and 0.2 NaGTP, pH 7.3, 295–300 mOsm. The data were acquired and processed (filtered at 2 kHz; digitized at 10 kHz) using Digidata 1440A, Multiclamp 700B, and Clampex 10.4 software (Molecular Devices). Only neurons with a resting membrane potential of less than –45 mV were used for further analysis. An optic fiber (200 µm in diameter) was carefully positioned above the brain slices. The eEPSCs were recorded by applying 473 nm light stimulation (30 mW, 5 ms duration; light in solution) to the axonal terminals of OVLT<sup>Glut</sup> neurons transfected with ChR2 in the PVN. Simultaneously, eEPSCs were recorded from PVN neurons that innervate the preBötC. The membrane potential was held at –65 mV during recording. To isolate monosynaptic connections, eEPSCs were recorded in the presence of TTX (1 µM), 4-AP (100 µM). The CNQX (10 µM) were perfused with aCSF to examine the neurotransmitter type used by ChR2-expressing OVLT<sup>Glut</sup> neurons.

To verify the reliability of optogenetic inhibition, we recorded neuronal firing in acute brain slices using cell-attached patch configuration. After inducing increased firing rates with hypertonic aCSF (160 mM Na<sup>+</sup>), we tested if yellow light (30 mW, 10 Hz; light in solution) could halt the rise in firing frequency.

### Immunohistochemistry and RNAscope

After administering anesthesia (urethane, 1.8 g/kg, i.p.), the mice were transcardially perfused with chilled saline for 5 min, followed by perfusion with 4% phosphate-buffered paraformaldehyde (PFA) (0.1 M, pH 7.4) for 20 min using a peristaltic pump operating at a flow rate of 2 mL/min. Whole brain was dissected and post-fixed at 4°C for 48 h. After that, it was washed with PBS, dehydrated in 30% sucrose in PBS at 4°C for at least 2 days, imbedded in blocks of 30% sucrose/OCT compound (1:1 mixture) and frozen at –80°C. Coronal sections (25 µm thickness) were obtained from the frozen brain blocks embedded in OCT compound using a cryostat device (Leica 1200s). The sections were blocked in 5% bovine serum albumin (BSA) in PBS (0.25% Triton X-100 in PBS) for 30 min at room temperature (23°C–24°C), followed by incubation with primary antibodies in 2% BSA-PBS overnight at 4°C. The sections were then washed three times with PBS again, and then incubated with secondary antibodies for 2 h at room temperature while protected from light. Finally, the sections were mounted with an anti-fluorescence quencher, and images were acquired with a fluorescence microscope (Zeiss, Germany) or a confocal laser-scanning microscope (LSM700, Zeiss). Immunolabelled neurons were counted using ImageJ. Source of antibodies and their dilutions were provided in key resources table.

To quantify cFos expression in the OVLT, MnPO, and SFO regions induced by 2 M NaCl or saline, coronal sections from each mouse (OVLT: 4 coronal sections, bregma +0.50 to +0.62 mm, 25 µm thickness, each separated by 25 µm; MnPO: 4 coronal sections, bregma +0.13 to +0.43 mm, 25 µm thickness, each separated by 75 µm; SFO: 8 coronal sections, bregma –0.81 to –0.11 mm, 25 µm thickness, each separated by 75 µm) were imaged at 10X magnification. The number of cFos-positive cells was then counted in ImageJ (NIH). Brain region locations were referenced from *The Mouse Brain in Stereotaxic Coordinates, 4th Edition*.

Fluorescent *in situ* hybridization was conducted using the RNAscope Multiplex Fluorescent Reagent Kit V2 from ACDBio in accordance with the manufacturer's instructions. Briefly, the brain tissue in OCT was sectioned into a thickness of 13 µm. To combine immunohistology with RNA-scope, the instructions were followed up to the hydrogen peroxide wash, then the sections were washed in PBS and incubated at 4°C overnight with the primary antibody diluted in Co-Detection Antibody Diluent (obtained from ACDBio). The sections were washed in PBS and treated with Protease Plus. The RNAscope protocol was then continued, the sections were washed in Wash Buffer Reagents (obtained from ACDBio) and incubated with the secondary antibody goat polyclonal secondary antibody diluted in Co-Detection Antibody Diluent for 30 min at room temperature. Finally, the sections were washed in PBS and mounted with Fluoromount-G from SouthernBiotech.

**QUANTIFICATION AND STATISTICAL ANALYSIS**

Statistical analysis was performed using Excel (Microsoft) and GraphPad Prism 9 software. Adobe Illustrator was used to compile figures for presentation. All data are presented as the mean  $\pm$  SEM. Differences between two groups were assessed using a two-sided Student's t-test. Multiple groups were compared using one- or two-way ANOVA followed by Bonferroni's or Tukey's multiple comparisons tests.  $p < 0.05$  was considered statistically significant.